Quaternary Science Reviews 324 (2024) 108376

Contents lists available at ScienceDirect

Quaternary Science Reviews

journal homepage: www.elsevier.com/locate/quascirev

Cryptotephra preserved in Lake Suigetsu (SG14 core) reveals the eruption timing and distribution of ash fall from Japanese volcanoes during the Late-glacial to early Holocene

Paul G. Albert [a,b,*], Danielle McLean [a,b], Hannah M. Buckland [a], Takehiko Suzuki [c], Gwydion Jones [a], Richard A. Staff [d], Sophie Vineberg [b], Ikuko Kitaba [e], Keitaro Yamada [e], Hiroshi Moriwaki [f], Daisuke Ishimura [c], Ken Ikehara [g], Christina J. Manning [h], SG14 Project Members[1], Takeshi Nakagawa [e], Victoria C. Smith [b]

[a] Department of Geography, Swansea University, Singleton Park, SA2 8PP, UK
[b] School of Archaeology, University of Oxford, Oxford, OX1 3QY, UK
[c] Department of Geography, Tokyo Metropolitan University, Minamiosawa, Hachioji, Tokyo, Japan
[d] Scottish Universities Environmental Research Centre, University of Glasgow, Scottish Enterprise Technology Park, East Kilbride, G75 0QF, UK
[e] Research Centre for Palaeoclimatology, Ritsumeikan University, Kusatsu, 525-8577, Japan
[f] Kagoshima University, 1-21-30 Korimoto, Kagoshima, 890-0065, Japan
[g] Research Institute of Geology and Geoinformation, Geological Survey of Japan, AIST, Tsukuba, Japan
[h] Department of Earth Sciences, Royal Holloway, University of London, Egham, Surrey, TW20 0EX, UK

ARTICLE INFO

Handling Editor: Giovanni Zanchetta

Keywords:
Ash fall
Cryptotephra
Lake Suigetsu
Tephrochronology
Japan
Late-glacial
Palaeoclimate
Archaeology
Asama
Sakurajima

ABSTRACT

Long sedimentary successions extracted for palaeoclimate research regularly preserve volcanic ash (tephra) fall from explosive eruptions and are increasingly used to elucidate the timing and scale of past events. This study investigates the non-visible tephra (cryptotephra) layers preserved in the annually laminated and intensively ^{14}C dated sediments of Lake Suigetsu (SG14 core), Japan. The cryptotephra investigations reported here focus on the Late-glacial to early Holocene sediments that were deposited between two visible tephra layers, the Ulleungdo (U)-Oki (10.2 ka) and the Sambe 'Sakate' (19.6 ka), and consequently span an interval of abrupt climate change making any newly identified cryptotephra layers invaluable chrono-stratigraphic markers. Using major and trace element volcanic glass compositions the cryptotephra are used to assign provenance to chrono-stratigraphically relevant eruption units. Five new cryptotephra layers are identified within this time interval. Three cryptotephra layers are from Kyushu volcanoes (SG14-1337 and SG14-1554 [Sakurajima]; and SG14-1806 [Kirishima]), all of which offer important chronological constraints on archaeological (Jomon) cultural transitions in southern Japan during the last termination. Another cryptotephra (SG14-1579), is assigned to activity on Niijima Island providing the first known distal occurrence and age of the eruption. Finally, the SG14-1798 cryptotephra precisely dated at 16,619 ± 74 IntCal20 yrs BP (2σ) is linked to Asama (As) volcano and more precisely the later phases of the As-YKU eruption. This discovery greatly expands the distribution of ash fall from this multi-phased eruption at Asama volcano, which affected an area in the region of 120,000 km^2. Refining the timing of the eruption and the distribution of As-YKU ash fall is important as it offers an excellent chrono- and climato-stratigraphic marker suitable for assessing spatial variability in environmental response to past climate change during the termination of the last glacial.

1. Introduction

Long sedimentary successions extracted for palaeoclimate research routinely preserve widely dispersed ash (tephra) fall deposits associated with past explosive volcanic eruptions. These tephra layers preserved either visibly and non-visibly (cryptotephra) provide essential chrono-

* Corresponding author. Department of Geography, Swansea University, Singleton Park, SA2 8PP, UK.
E-mail address: p.g.albert@swansea.ac.uk (P.G. Albert).
[1] www.suigetsu.org.

https://doi.org/10.1016/j.quascirev.2023.108376
Received 1 June 2023; Received in revised form 21 October 2023; Accepted 22 October 2023
Available online 2 December 2023
0277-3791/© 2023 The Authors. Published by Elsevier Ltd. This is an open access article under the CC BY license (http://creativecommons.org/licenses/by/4.0/).

stratigraphic markers capable of both synchronising (tephrostratigraphy) and dating (tephrochronology) disparate palaeoclimate archives, which facilitate the assessment of spatio-temporal variations in past climate change (e.g., Lowe et al., 2012; Lane et al., 2013). Simultaneously, distal tephra archives can have independent and precise chronologies (e.g., radiocarbon dating [^{14}C], annual layering [varve]) that are increasingly being used to elucidate the timing, recurrence and extent of ash fall events associated with past eruptions, crucial to informing more reliable volcanic reconstructions and hazard assessments (e.g., Albert et al., 2013, 2015, 2018; Kutterolf et al., 2008; Sulpizio et al., 2014).

Here we aim to identify and capitalise upon non-visible tephra (cryptotephra) layers preserved in the robustly dated (via ^{14}C) and annually laminated (varved) Late-glacial to early Holocene sediments of the globally renowned palaeoclimate archive, Lake Suigetsu, central Honshu Island, Japan (e.g., Nakagawa et al., 2021). The period extending from the Late-glacial to the early Holocene (the last termination) is particularly significant from both a palaeoclimate and archaeological perspective. It is punctuated by numerous globally traced abrupt and large amplitude climatic transitions (e.g., Clarke et al., 2002; Alley et al., 2003). The timing and scale of Late-glacial climatic instabilities in Japan are very well resolved by pollen-based temperature reconstructions at Lake Suigetsu (e.g., Nakagawa et al., 2021), and provide the backdrop for cultural changes in Japan associated with hunter-gatherer and Jomon sedentary societies (e.g., Nakazawa et al., 2022). Consequently, developing the Late-glacial tephrostratigraphy of a Lake Suigetsu is key to better constraining the timing and synchroneity of these transitions.

Lake Suigetsu is known to preserve a detailed visible tephrostratigraphy (>30 layers) spanning approximately the last 150 ka. Numerous calc-alkaline (CA) to high-K calc-alkaline (HKCA) tephra layers are correlated to productive Japanese volcanic sources located to the south within the southern (e.g., Kikai, Ata, Aira) and central (e.g., Aso, Kuju) Kyushu volcanic regions (e.g., Smith et al., 2013; Albert et al., 2019). Dominant sources of visible tephra deposits include the two nearby and upwind stratovolcanoes of Daisen and Sambe situated along the South-West Japan Arc (SWJA; Albert et al., 2018, Fig. 1). While alkali-rich tephra deposits are traced to explosive volcanism beyond Japan at intra-plate volcanoes Changbaishan (North Korea/China border) and the South Korean island of Ulleungdo in the Sea of Japan (e.g., McLean et al., 2016, 2020b).

Crucially, cryptotephra investigations targeting the Lake Suigetsu sediments spanning other time-intervals (0–10 ka and 30–50 ka) have revealed four times more cryptotephra deposits relative to visible tephra

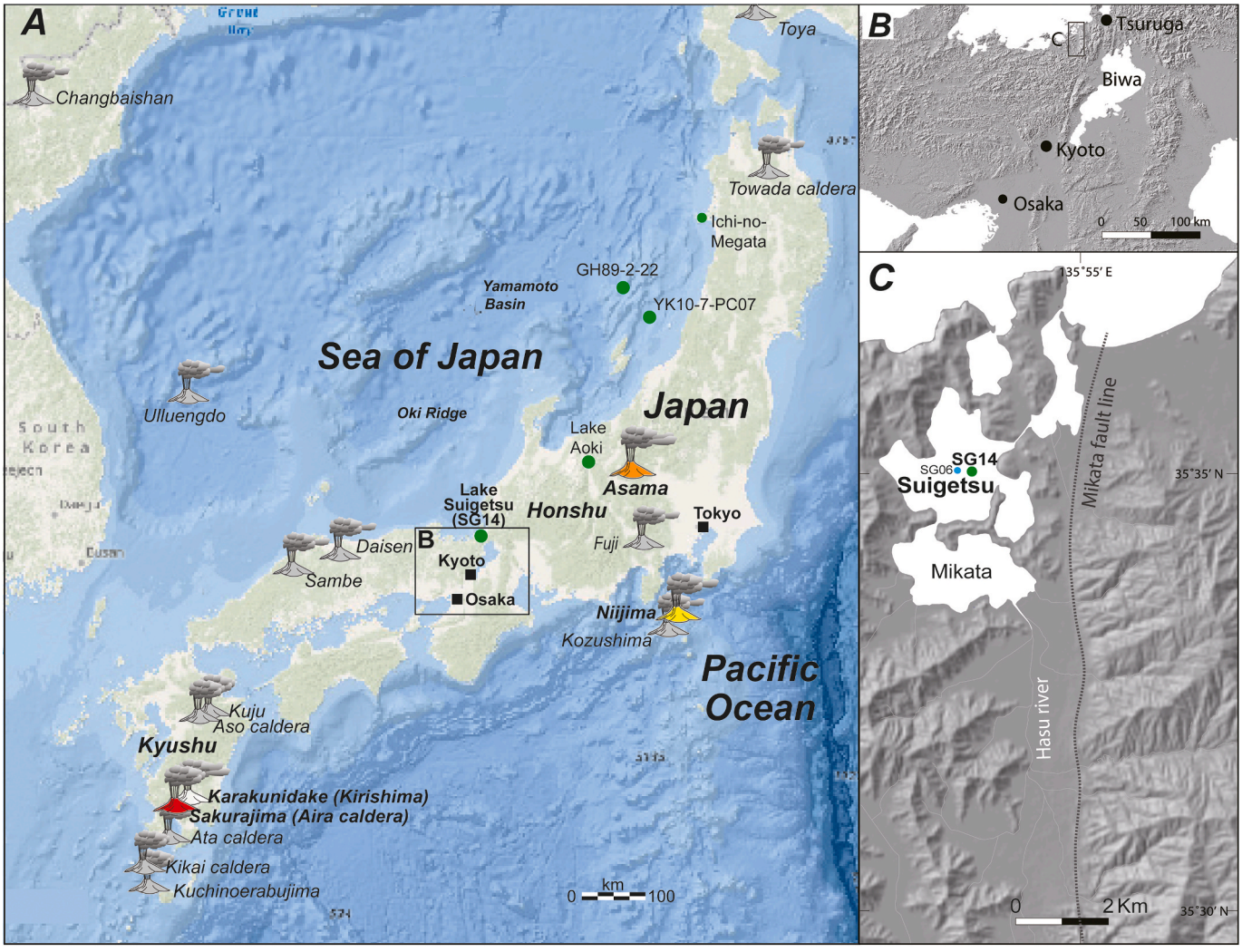


Fig. 1. (A) A map showing the location of Lake Suigetsu, central Honshu Island, Japan, relative to potential volcanic sources of the cryptotephra layers identified. Chrono-stratigraphically relevant eruption units at the volcanoes marked in bold have been the focus of new chemical characterisation. (B) A map showing the location of Lake Suigetsu north-west of Lake Biwa; (C) map showing Lake Suigetsu as the largest of the Five Mikata Lakes which are located immediately adjacent to the Wakasa Bay, Sea of Japan. The position of the coring campaigns SG06 and SG14 are marked on Lake Suigetsu (B and C modified from Nakagawa et al., 2005).

(e.g., McLean et al., 2018). These findings have provided precise age constraints on past eruptions and enabled the integration of regional tephrostratigraphies spanning the full length of the Japanese islands, even provided the first tephra linkage between Lake Suigetsu and the Greenland ice cores (B-Tm; –Sun et al., 2014; McLean et al., 2016). The expansion of the Lake Suigetsu tephrostratigraphy through cryptotephra analysis acts to cement the site as a central node within a tephrochronological framework of East Asia (e.g., McLean et al., 2018, 2020a) and demonstrates the enormous benefits of resolving additional tephrochronological and volcanological information from within Late-glacial to early Holocene sediments at Lake Suigetsu.

The specific objectives of this contribution are to; (i) correlate the identified Late-glacial to early Holocene cryptotephra deposits to known eruptions in order to further constrain the distribution of widespread ash fall events; (ii) provide high-precision independent eruption ages using the Lake Suigetsu chronology; and (iii) develop an integrated tephrostratigraphic framework within the context of an important interval of climatic and archaeological change, suitable for synchronising and dating regional records, and exploring links to other globally significant archives (e.g., Greenland ice cores).

2. Explosive volcanism in and around Japan during the Late-glacial to early Holocene

Japan has over 130 volcanic centres, relating to the complex interaction and subduction of multiple tectonic plates. Principally, the Philippine Sea Plate is subducted along the Ryukyu-Kyushu Arc and the SWJA, while the Pacific Plate is subducted along the NE Japan Arc (NEJA) and the Kurile Arc. Many of these centres have been highly productive during the Late Pleistocene and Holocene. Calderas and intra-caldera volcanism dominate in Kyushu, northern Honshu and Hokkaido, and volcanoes in these regions are responsible for some of the largest explosive eruptions known globally during the Late Quaternary (Machida, 1999; Machida and Arai, 2003).

Near-source Japanese eruption records indicate the Late-glacial to early Holocene period is punctuated by some large Magnitude (M) volcanic eruptions (> M 5.0), while M 4.0 or Volcanic Explosivity Index (VEI) 4 sub-Plinian to Plinian eruptions are more frequently reported (Table 1). The largest eruption during this interval is the M 6.7 Towada Hachinohe (To-H) caldera-forming eruption in northern Honshu (Fig. 1). The eruption produced phreato-Plinian fall deposits, interbedded with pyroclastic density current (PDC) deposits, which culminated with the emplacement of the thick Hachinohe Ignimbrite (Hayakawa, 1985). More than 50 km^3 of tephra was erupted and predominantly dispersed to the east (Hayakawa, 1985), with ash fall being traced well into the Pacific Ocean (e.g., Ikehara et al., 2013, 2017). Bourne et al. (2016) suggested that this eruption is preserved as a cryptotephra layer in the Greenland ice core NEEM which is dated at 15,706 ± 226 yrs b2k. The Greenland derived age is in broad agreement with a re-calibrated (^{14}C) age estimate of material buried in the To-H eruption deposits, 15,615–15,895 IntCal20 yrs BP (Muscheler et al., 2020).

The Asama (As) stratovolcano located in central Honshu (Fig. 1), produced a highly explosive multi-phased eruption during the Late-glacial. Two Plinian eruption deposits are traced south-east (Asama Itahana Yellow Pumice; As-YP), and north-east (Asama Kusatsu Pumice [or Tsumagoi]; As–K) of the volcano, respectively. Different authors have classified the eruption as a VEI 5 (Machida and Arai, 2003) and M 6.5 (Hayakawa, 2010) eruption. PDC's associated with the eruption, specifically the Komoro pumice flow deposits, have been traced to south and to the north-east of the volcano. Radiocarbon dating of tree stumps buried in this As-YP unit have an age range of 15,620–17,040 IntCal20 yrs BP (Nakamura et al., 1997). There is no reported evidence of a significant eruptive hiatus (e.g., palaeosol) between the Plinian deposits and it is thought that a co-PDC ash dispersal might be responsible for the reported distal occurrence of the Asama Upper Glass (As-UG), west of Tokyo and away from the two main Plinian dispersal axis (Machida and Suzuki, in press). Subsequently, the combined activity is grouped as the As-YKU in Japanese eruption/tephra catalogues (e.g., Hayakawa, 2010; Machida and Suzuki, in press). Sakurajima (Sz) stratovolcano, situated in southern Kyushu on the southern edge of Aira caldera (Fig. 1), formed by the Aira Tanzawa (AT) super-eruption (and preceding events), has produced sub-Plinian to Plinian eruptions during the interval of interest, the largest being associated with the Satsuma (Sz-S) Plinian pumice fall beds, and this event saw an estimated 11 km^3 of tephra erupted (Kobayashi and Tameike, 2002), equating to a M 5.9 event (Hayakawa, 2010).

3. Study site (Lake Suigetsu)

Lake Suigetsu, central Honshu Island (35°35′0″N, 135°53′0″E) is located in a small tectonic basin situated on the western side of the Mikata fault line, adjacent to Wakasa Bay (Fig. 1). It covers an area of ~4.3 km^2, has an average water depth of approximately 34 m and represents the largest of the 'Mikata Five Lakes'. The small catchment of the lake is vegetated by warm mixed-forest and is bound by a ring of Palaeozoic hills (maximum elevation 400 m) (Kitagawa et al., 1995; Nakagawa et al., 2005). The Hasu River enters the neighbouring Lake

Table 1
Reported Late-glacial to early Holocene explosive eruptions at Japanese and Izu arc volcanoes which are considered as Magnitude (M) 4.0 or Volcanic Explosivity Index (VEI) 4 events or greater, and are therefore likely near-source equivalents of distal tephra deposits preserved in the temporally relevant sediments of Lake Suigetsu, central Honshu, Japan. References (1) Moriwaki et al. (2011); (2) Hayakawa (2010); (3) Okuno et al. (1997); (4) Kobayashi and Tameike (2002); (5) Moriwaki et al. (2017); (6) Okuno (1997); (7) Imura (1992); (8) Nagaoka et al. (2010); (9) Moriwaki et al. (2016); (10) Machida and Arai (2003); (11) Hayakawa (1985); (12) Muscheler et al. (2020); (13) Nakamura et al. (1997); (14) Kobayashi et al. (2020).

Region	Source Volcano	Eruption	Tephra	M	VEI	Volume (km^3)	Dispersal	Age	Refs
Kyushu	Kuchinoerabujima (Noike; N)	Yumugi	N-Ym	5.3	6	0.6	E (L,M) and W (U)	14,525–15,245	1, 2
Kyushu	Sakurajima (Sz)	Uwaba/Pumice 12	Sz-Ub	4.0	–	0.3	E	9135–9525	2, 3, 4
	Sakurajima (Sz)	Takatoge 3/Pumice 13	Tk3	4.0	4	1.3	E	10,585–11,175	2, 3, 4
	Sakurajima (Sz)	Satsuma/Pumice 14	Sz-S	5.9	5	11	Radial. SW	12,755–13,760	2, 3, 4
	Aira (A)	Shinjima/Moeshima		4.0	–	–	–	~13,000	2, 4, 5
	Aira (A)	Takano Base surge	A-Tkn	–	–	–	E	18,215–18,785	5, 6
Kyushu	Ko-Takachiho, Kirishima (Kta)	Kamamuta	Kr-Km	5.0			–	~8.1 ka	2, 7
	Shinmoedake, Kirishima (Sh)	Setao	Kr-St		4?	0.07	–	~10.4 ka	2, 7, 10
	Karakunidake, Kirishima (Kr)	Kobayashi	Kr-Kb	5.2	5	0.91	NE	~16,700 ka	2, 7, 8, 10
Honshu	Towada	Hachinohe Ignimbrite	To-H	6.7	6	50	Radial (E)	15,615–15,895	2, 10,11, 12
	Towada	Hachinohe Pumice	To-HP				E		
Honshu	Asama	'Tachikawa' Upper Glass	UG	6.5	5	?	co-PDC?	15,620–17,040	2, 10, 13
	Asama	Katsatsu Pumice	As–K				N (E)		
	Asama	Itahana Yellow Pumice	As-YP				E (S)		
Izu Arc	Niijima	Miyatsuka-yama	Nj-Mt (Nj-MtG)	4.8	4	0.7	SE	10,700–13,200	14

Table 2
Summary table of tephra layers within the Late-glacial to early Holocene sediments of Lake Suigetsu (SG06/SG14 cores). Visible layers previously reported are in bold, with references for correlations to volcanic source and eruption units being * Smith et al. (2013) and ** Albert et al. (2018).+SG14-1185 was reported in McLean et al. (2018). V/C = **Visible**/Cryptotephra. V= Vesicular; MV = Micro-vesicular; F = Fluted, MI = Microlite Inclusions; C = Cuspate; BW =Bubble walled.

SG14 label	V/C	SG14 Master core and position	SG14 CD (cm) (ver.Feb 28, 2019)	SG06 CD (cm) (ver.Apr 06, 2020)	IntCal20 yrs BP (median ± 2s)	Shards/gram	Glass shard Morphology	Shard long axis (μm)	Correlation based on glass geochemistry (volcano, tephra)	Magnitude (M)*	Source to Suigetsu (km)
+SG14-1185	C	F-12 (62.0–63.0 cm)	1184.0–1185.0	1180.33–1181.34	9,337 ± 34	>5000	MV, MI	40–50	Shinmoedake (Kirishima), Seto (Kr-St)?	–	620
SG06–1288	**V**	**G-03–02 (34.3–32.2)**	**1301.3**	**1287.9**	**10,196 ± 32**	**-**	**MV**	**60**	**Ulleungdo, U4** *	**6.7**	**495**
SG14-1337	C	F-14 (36.0–37.0 cm)	1335.7–1336.7	1330.47–1331.59	10,623 ± 50	2983	V, F	80–100	Sakurajima, Tk-3 (Pumice 13)	4.0	650
SG14-1554	C	F-16 (55.0–56.0 cm)	1552.6–1553.6	1567.22–1568.25	12,922 ± 58	10,983	MV, MI	100	Sakurajima, Unknown	-	650
SG14-1579	C	E–17 (53.0–54.0 cm)	1577.9–1578.9	1595.13–1596.28	13,320 ± 64	6959	F, PV	100	Nijima-Miyatsuka-yama (Nj-Mt/Mt)	4.8	335
SG14-1798	C	G-04 (49.0–50.0 cm)	1797.3–1798.3	1805.33–1806.22	16,619 ± 74	2043	C (BW)	60	Asama, Y/K/U	6.5	248
SG14-1806	C	G-04 (57.0–58.0 cm)	1805.3–1806.3	1812.40–1813.28	16,789 ± 72	2558	MV, MI	120	Karakunidake (Kirishima), Kobayashi (Kr-kb)	5.2	620
SG06–1965	**V**	**E-21 (54.2–54.9 cm)**	**1950.8**	**1964.5**	**19,645 ± 80**	**-**	**MV, B**	**100**	**Sambe, Md-fl/Sakate** **	**5.8**	**305**

Mikata, with water flowing through into Lake Suigetsu via the Seto Channel. The shallow channel connecting the lakes, acts as a coarse-grain sediment filter, making the sedimentary environment of Lake Suigetsu particularly stable, and dominated by fine-grained deposition. The Lake Suigetsu sediments have been studied for over three decades, with the 'SG93' coring campaign driving great interest in the site. The SG93 coring revealed that a significant portion of the sedimentary succession contained varves ('nenko' in Japanese), with seasonal laminations alternating between diatom rich (dark) and mineral-rich (light) layers (Kitagawa et al., 1995; Kitagawa and van der Plicht, 1998a; Nakagawa et al., 2003).

The lake was re-drilled in 2006 as part of the 'Lake Suigetsu Varved Sediment Project' with the aim of obtaining a complete 'master' sedimentary sequence by recovering overlapping cores from four parallel boreholes (A, B, C and D, situated ~20 m apart). The campaign successfully extracted a 73.40 m-long composite core ('SG06'), providing a continuous record of sedimentation spanning at least the last 150 ka (Nakagawa et al., 2012). The sequence is varved between ~10 and 70 ka, and the sediments have been intensively radiocarbon (^{14}C) dated, and layer counted, to generate a high-resolution chronology (Staff et al., 2011; Bronk Ramsey et al., 2012; Marshall et al., 2012; Schlolaut et al., 2012, 2017; Nakagawa et al., 2021). A new coring campaign was undertaken during the summer of 2014 to obtain another continuous core sequence. The coring site was located ~320 m east of the SG06 boreholes (Fig. 1b) and was similarly obtained using a hydro-pressure piston sampler, and a triple sampler for deeper parts. This campaign retrieved a composite overlapping sedimentary sequence from four boreholes (E, F, G and H) spanning ~98 m, which records ~25 m of additional sedimentation compared to SG06, reaching a thick basal gravel. This composite master sequence, named 'Fukui-SG14' ('SG14' in short), was used for this cryptotephra investigation. The SG14 sequence (correlation model 30 May '17) has been precisely tied to the SG06 composite core (correlation model 08 May '16) using 361 common marker layers (which include visible tephra layers), the same approach used to correlate the core sections of the different SG06 boreholes (as outlined in Nakagawa et al., 2012), permitting the high-precision SG06 chronology to be transferred to the SG14 core.

4. Methods

4.1. Cryptotephra identification

For continuity, SG06 labelling codes are used for the visible tephra bracketing this interval of cryptotephra investigation within the SG14 core. The SG14 master core (composite sequence) was contiguously subsampled at a ~5 cm (low-) resolution, from the Ulleungdo - U-Oki (SG06-1288; Smith et al., 2011; Smith et al., 2013) tephra down to the Sambe – Sakate (Md-fl; SG06-1965; Albert et al., 2018), avoiding known visible high-energy event layers (e.g., flood horizons). Where elevated shard concentrations were observed and unrelated to an underlying visible tephra (e.g., SG06-1965), the sediment was resampled at a 1 cm (high-) resolution to determine the precise stratigraphic positioning of the cryptotephra peak within the 5 cm sample. During intervals chrono-stratigraphically relevant to well-known and widespread tephra markers (e.g., To-H, Sz-S), 1 cm resolution counting was conducted even in the absence of low-resolution peaks to maximise the possibility of their identification.

All samples were wet sieved through a 25 μm nylon mesh a 80 μm mesh was not required owing to the very fine-grained nature of the sediments. The retained >25 μm fraction was subject to heavy liquid density separation (Turney, 1998; Blockley et al., 2005) to extract the volcanic glass shards. This stepped floatation method is shown to reliably resolve cryptotephra peaks, even those containing low glass concentrations (e.g., <500 shards/gram) in the Lake Suigetsu sediments, where peaks that would not have been detected using other techniques such as μXRF core scanning (e.g., McLean et al., 2022). The extracted

material was subsequently mounted on slides using Canada Balsam, and glass shards were counted using a light microscope. Shard concentrations are quantified as shards per gram of dried sediment (shards/gram).

The criteria used to (morphologically and geochemically) classify glass shards, and decipher primary cryptotephra layers versus reworked layers follows those outlined in McLean et al. (2018) based on the examination of Holocene Lake Suigetsu sediments. We find a constant, yet variable glass shard concentration associated with the 30 ka Aira

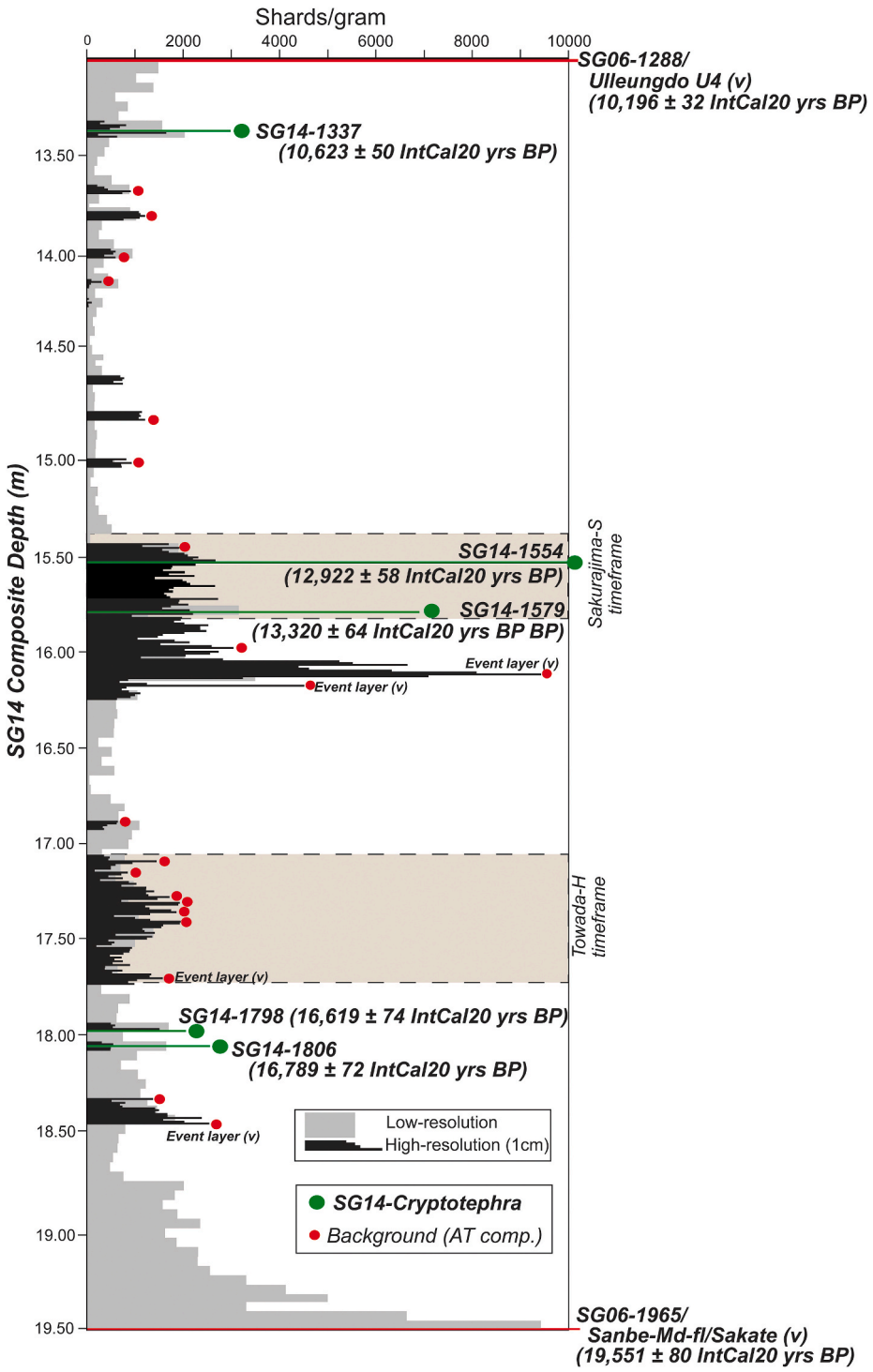


Fig. 2. Glass shard concentrations spanning the early-Holocene and Late-glacial sediments of the Lake Suigetsu SG14 core. The shards per gram of dried sediment, which are capped at 10,000 shards) The interval investigated is bracketed by visible tephra layers, SG06-1288/U-Oki and SG06-1965/Sambe-Md-fl/'Sakate'. Concentrations of glass shards in low-resolution (5 cm interval) samples are shown in grey, whilst high-resolution (1 cm) sample are overlain in black. Green 1 cm intervals represent the five cryptotephra peaks where geochemically distinctive layers are identified. Depth scale is based on SG14 composite depth (See text). Shaded brown intervals represent the broad age-range of two widespread Japanese eruption units, Towada-Hachinhoe (To-H), and Sakurajima-Satsuma (Sz-S), where detailed high-resolution cryptotephra analysis was conducted irrespective of low-resolution shard counts. Red dots denote where chemical analysis were conducted but analyses were consistent with the AT tephra (i.e., Background glass). (v) denotes a *visible* event layers in the core, which often relate to flood events, or in the case of SG06-1288 and SG06-1965 are visible tephra layers (tephra fall events). Lake Suigetsu IntCal20 ages are reported ±2 standard deviations.

caldera-forming eruption (AT tephra) throughout the Late-glacial sedimentary profile at Lake Suigetsu, which we classify as '*background*' glass within these sediments. Evidently, glass shards from this Magnitude 8 eruption are frequently remobilised in the Suigetsu catchments and washed into the lake. However, they are easily identified via their platy morphology and chemical composition, and most clearly peak during higher energy events (e.g., floods). We also checked for possible 'cryptic' reworking events using the high-resolution μXRF core scanning data following the criteria outlined in McLean et al. (2022). Consequently, where chemically distinct primary cryptotephra peaks are identified, we also chemically observe a minor AT background. The observed sub-populations of AT glass shards, and AT laden in-wash events, are discounted as primary ash fall layers (chemical data can be found in Supplementary Material 2; Fig. 2).

Immediately above visible tephra SG06-1965 (Sambe-Md-fl) sediments spanning 19.50 and 18.75 m SG14 Composite Depth (CD) revealed elevated shard concentrations in the low-resolution sampling and are above 2000 shards/gram. The glass shards were morphologically consistent with the underlying tephra (SG06-1965), a feature observed above other visible tephra deposits in Lake Suigetsu (e.g., K-Ah; McLean et al., 2018). Consequently, high-resolution investigations began once concentrations had dropped back below 1000 shards/gram (Fig. 2).

4.2. Chemical characterisation

Glass shards were extracted from SG14 cryptotephra samples chosen for geochemical analysis and hand-picked from a well-slide using a micromanipulator (see Lane et al., 2014). The shards were mounted in *Struers* Epoxy resin stubs, which were sectioned to expose a flat surface, then polished using diamond paste (3 and 1 μm), and finally carbon coated for chemical analysis.

Major and minor element compositions of individual glass shards were measured using a JEOL-8600 wavelength-dispersive electron microprobe (WDS-EMP) at the Research Laboratory for Archaeology and History of Art (RLAHA), University of Oxford. A beam accelerating voltage of 15 kV was used with a 6 nA current and a defocused beam diameter of 10 μm. The instrument was calibrated with a suite of appropriate mineral standards; peak count times were 30 s (s) for all elements except Mg (50s), Mn (50s), Na (10s), Cl (50s), and P (50s). Reference glasses from the Max Plank institute (MPI-DING suite; Jochum et al., 2006) were also analysed alongside the tephra. These included felsic [ATHO-G (rhyolite)], through intermediate [StHs6/80-G (andesite)] to mafic [GOR132-G (komatiite)] glasses. Accuracies of analyses on these MPI-DING glasses are typically 0.2 wt%; the data become more qualitative for those elements with concentrations <0.2 wt%. Errors are typically $< \pm$ 0.5% RSD for Si; $< \pm$ 4% for most other major elements, except for the lower abundance elements: Ti, Mn, P and Cl.

Trace element analysis of volcanic glass shards from the SG14 cryptotephra deposits and near-source reference material were performed using an Agilent 8900 triple quadrupole ICP-MS (ICP QQQ) coupled to a Resonetics 193 nm ArF excimer laser-ablation in the Department of Earth Sciences, Royal Holloway, University of London. Spot sizes of 20, 25 and 34 μm were used depending on the sample vesicularity and/or size of glass areas available for analysis. The repetition rate was 5 Hz, with a count time of 40 s on the sample, and 40 s of the gas blank to allow the subtraction of the background signal. Typically, blocks of eight or nine glass shards and one MPI-DING reference glass were bracketed by the NIST612 glass adopted here as the calibration standard. The internal standard applied was ^{29}Si (determined by EMP-WDS analysis). In addition, the same MPI-DING referenceglasses listed above were used to monitor analytical accuracy (Jochum et al., 2006). LA-ICP-MS data reduction was performed within Microsoft Excel following the protocols outlined in Tomlinson et al. (2010). Accuracies of LA-ICP-MS analyses of the MPI-DING reference glasses, ATHO-G and StHs6/80-G, were typically ≤5% for most elements measured.

All SG14 cryptotephra, near-source reference material, and standard measurements from both methods are provided in the Supplementary Material 1. Data averages are reported as $\pm$ 1 standard deviations, error bars on the trace element plots are typically smaller than the symbols.

4.3. Lake Suigetsu chronology

The master SG14 sequence was precisely aligned to the SG06 sequence using regular and distinctive marker horizons, permitting the high-precision SG06 chronology to be transferred to the SG14 core. SG06 event-free depth(s) (EFD, ver. 13th Feb '17) were used within the age model, which excludes instantaneous deposits >5 mm in thickness, i.e., event layers (Staff et al., 2011; Schlolaut et al., 2012). The software package developed to handle the correlation of parallel core sections, 'LevelFinder' (ver. 7.7.1, http://polsyems.rits-palaeo.com), was used to linearly interpolate between the common marker layers and determine any given composite depth (CD) or EFD from the individual SG06 and SG14 core sections.

Between 16.5 m (ca. 13,950 IntCal20 yrs BP) and 40.3 m SG06 composite depth (ca. 50,296 IntCal20 yrs BP), the Lake Suigetsu radiocarbon data are directly incorporated into the construction of the consensus IntCal calibration curve itself, therefore directly providing IntCal20 ages for this section of the composite Suigetsu sedimentary sequence (Bronk Ramsey et al., 2020; Reimer et al., 2020a). The upper sediments (i.e., younger than 13,950 IntCal20 yrs BP), for which the Lake Suigetsu ^{14}C data were not themselves incorporated into IntCal20, required resultant modelling on to the IntCal20 timescale (Reimer et al., 2020b). This was achieved through implementing two successive cross-referenced Poisson-process ('P_Sequence') depositional models using OxCal (ver. 4.4; Bronk Ramsey, 2008; Bronk Ramsey and Lee, 2013, Bronk Ramsey, 2022); the lower section (below 12.88 m SG06 CD) incorporated varve count data from Schlolaut et al. (2018), and the upper section (above 12.88 m SG06 CD), for which countable varves are not preserved, utilised EFD. In total, the Lake Suigetsu age model is therefore based upon 808 AMS ^{14}C dates obtained from terrestrial plant macrofossils from the SG93 and SG06 cores (Kitagawa and van der Plicht, 1998a, Kitagawa and van der Plicht, 1998b, Kitagawa and van der Plicht, 2000; Staff et al., 2011; Bronk Ramsey et al., 2012; Staff et al., 2013a; Staff et al., 2013b), 525 of which are directly included within the IntCal20 calibration curve itself (Bronk Ramsey et al., 2020). Modelled cryptotephra ages placed upon this IntCal20 timescale, represent the entire 1-cm depth interval, rather than the sub-sampling mid-point, and thus provide a truer reflection of the full chronological uncertainties, consistent with McLean et al. (2018).

4.4. Reference tephra samples (near-vent and distal)

To evaluate the probable source regions of the newly characterised Lake Suigetsu cryptotephra deposits, their glass signatures were compared to published Japanese volcanic glass reference datasets (e.g., Kimura et al., 2015; Albert et al., 2019). New reference pumice and ash samples for temporally relevant eruptions (Table 1) were collected and subject to major and trace element glass analysis. This involved analysis of near-vent samples from Asama, Sakurajima, Aira, Kirishima and Niijima volcanoes. We also analysed distal samples of reported Late-glacial Asama ash fall layers preserved and reported in other sediment cores (Okuno et al., 2011; Nagahashi et al., 2022). Full details of the newly sampled near-source units and distal ash layers are reported in the Supplementary Material 2. These samples were analysed under the same analytical conditions as the SG14 cryptotephra outlined in section 4.2.

5. Results

Five primary cryptotephra deposits are identified in the interval spanning between SG06-1965 and SG06-1288, with representative glass shards from each deposit shown in Fig. 3. These deposits all peaked

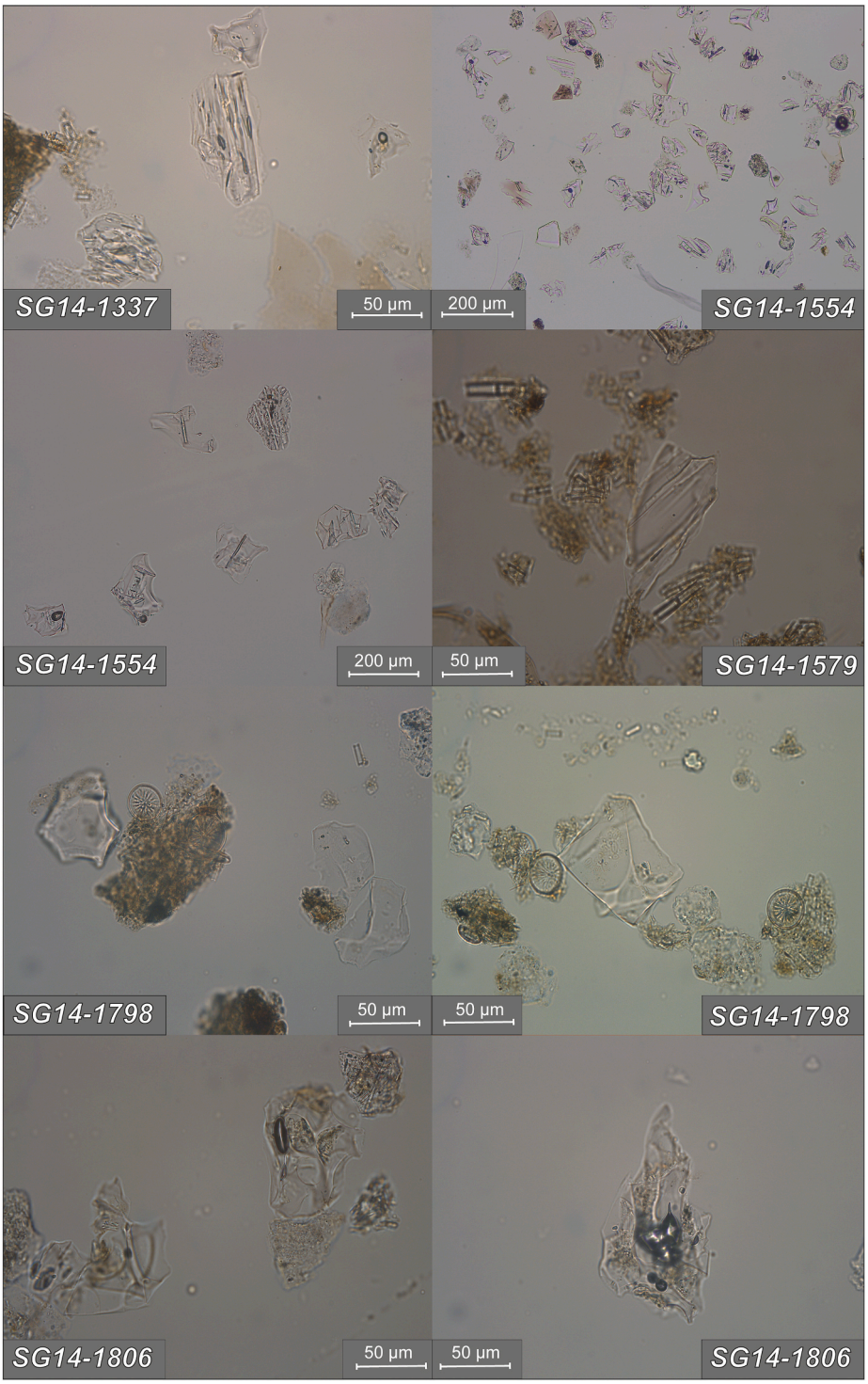


Fig. 3. Photographs of representative glass shards associated with the five cryptotephra layers identified in the early Holocene to Late-glacial sediments of Lake Suigetsu investigated here. Different cryptotephra have dominant shard morphologies (Table 2), for instance SG14-1806 are micro-vesicular and contain inclusions, whilst SG14-1798 display cuspate, bubble-wall features.

above 2000 shards/gram (Fig. 2; Table 2), and display a dominant glass composition that Table 2 can be distinguished from the AT glass background (See Section 4.1). The five newly identified cryptotephra layers are labelled herein using their SG14 composite depth in cm (SG14-CD, ver.Feb 28, 2019) rounded to the nearest integer (Table 2). They are SG14-1337, SG14-1554, SG14-1579, SG-14-1798, SG14-1806 and they are dated to 10,623 ± 50 IntCal20 yrs BP; 12,922 ± 58 IntCal20 yrs BP; 13,320 ± 64 IntCal20 yrs BP; 16,619 ± 74 IntCal20 yrs BP; and 16,789 ± 72 IntCal20 yrs BP (2σ) respectively, using the Lake Suigetsu IntCal20 chronology.

5.1. Cryptotephra glass chemistry

5.1.1. SG14-1337 (10,623 ± 50 IntCal20 yrs BP)

SG14-1337 has a relatively homogenous rhyolitic chemistry (71.9–73.7 wt% SiO_2 [$n = 22$]) which displays a medium-K (2.5–3.0 wt

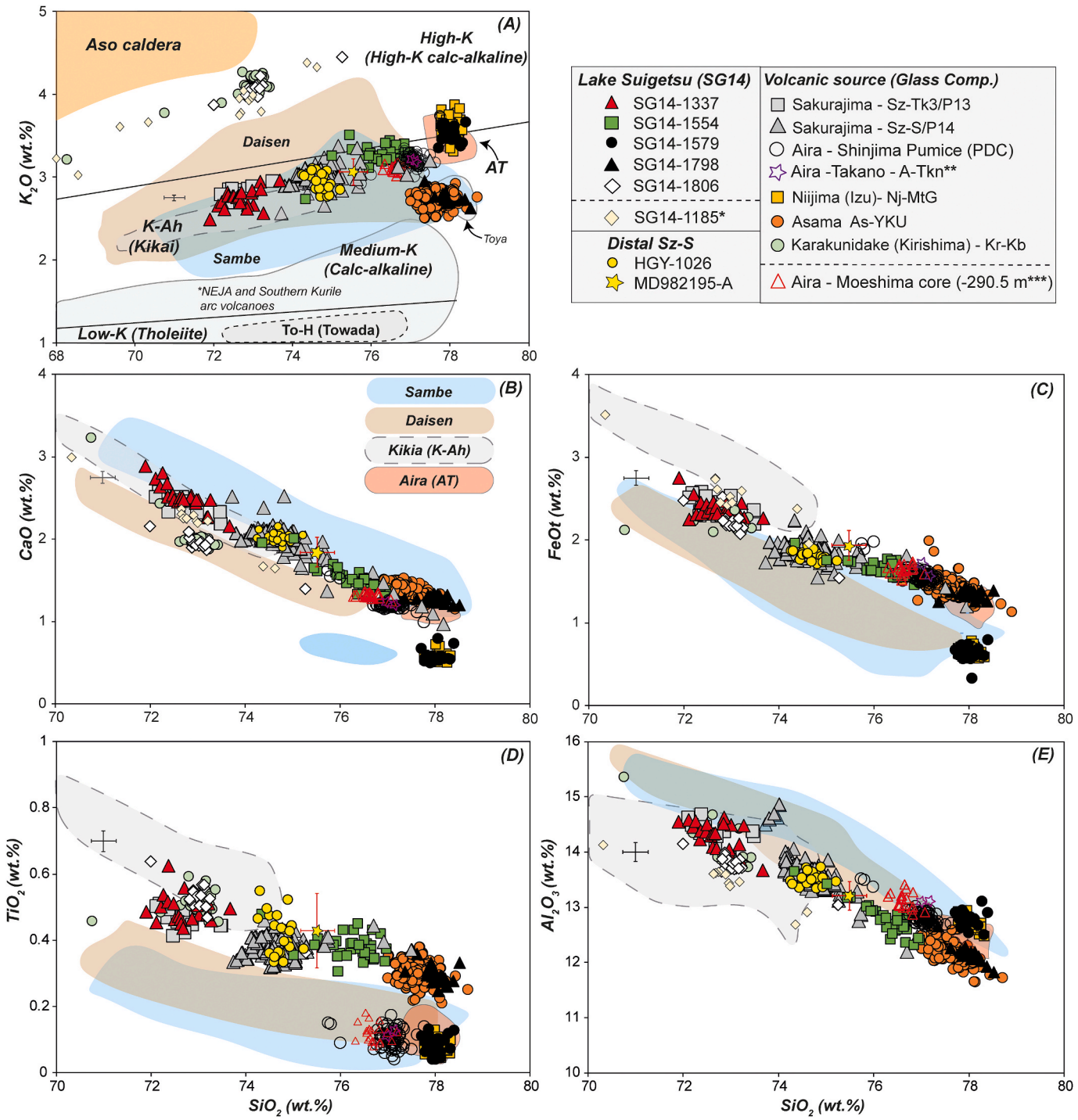


Fig. 4. Major element glass compositions of the cryptotephra layers in the early Holocene and Late-glacial SG14 sediments investigated compared to new reference chemical datasets produced for chrono-stratigraphically relevant eruption units at Sakurajima (Aira caldera), Karakunidake (Kirishima), Asama and Niijima volcanoes. (A) K_2O classification fields follow Peccerillo and Taylor (1976). Compositional fields/envelopes for Daisen and Sambe glasses are following data presented in Albert et al. (2018), whilst K-Ah (Kikai) and AT (Aira) compositional fields follow Smith et al. (2013). *SG14-1185 represents a previously un-assigned Holocene cryptotephra from Lake Suigetsu (McLean et al., 2018). **Reference compositions for the Aira Takano base surge (A-Tkn; Fukaminato) are from Moriwaki et al. (2017), ***while data for a possible correlative of the Takano base surge, identified at −290.5 m depth within a borehole core extracted on Moeshima island (below the Shinjima PDC deposits) are also shown, with data reported in the supplementary material 1. Error bars on plots represent reproducibility, and 2 standard deviations of replicate analysis of MPI-DING StHs6/80-G standard.

% K_2O) calc-alkaline affinity (Fig. 4A; Table 3). Using increasing SiO_2 content as a fractionation index CaO (2.2–2.9 wt%) and Al_2O_3 (14.6–13.7 wt%) decrease, and K_2O increases, while FeOt (2.4 ± 0.1 wt %) and Na_2O (4.1 wt%) remain relatively constant. The glasses are enriched in Rb relative to the High Field Strength Elements (HFSE), with a strong depletion in Nb and Ta (Fig. 5). The glasses are also enriched in Light Rare Earth Elements (LREE) relative to the Heavy Rare Earth Elements (HREE) where La/Yb_N = 5.5 ± 0.6 (1σ; Fig. 5). Incompatible trace element concentrations show limited variability (9.3 ± 0.5 ppm Th; 175 ± 9 ppm Zr; 26.9 ± 1.0 ppm Y [1σ; n = 8]; Fig. 6) consistent

Table 3
Average major (EMP) and trace element (LA-ICP-MS) volcanic glass chemistry of Lake Suigetsu Late-glacial to early Holocene cryptotephra deposits. Major element glass data has been normalised (water-free). Full geochemical datasets are available in the Supplementary Material 1.

Tephra	SG14-1337		SG14-1554		SG14-1579		SG14-1798		SG14-1806	
wt.%	Ave.	±1σ	Ave.	±1σ	Ave.	±1σ	Ave.	±1σ	Ave.	±1σ
SiO_2	72.70	0.43	76.17	0.55	78.00	0.18	78.01	0.25	73.08	0.63
TiO_2	0.50	0.04	0.37	0.04	0.08	0.03	0.29	0.03	0.53	0.06
Al_2O_3	14.30	0.26	12.75	0.33	12.77	0.13	12.16	0.16	13.77	0.23
FeOt	2.38	0.11	1.69	0.15	0.62	0.09	1.34	0.05	2.19	0.20
MnO	0.08	0.02	0.07	0.02	0.06	0.02	0.04	0.02	0.05	0.03
MgO	0.61	0.11	0.37	0.13	0.09	0.04	0.25	0.04	0.52	0.08
CaO	2.51	0.17	1.52	0.16	0.56	0.07	1.28	0.04	1.93	0.15
Na_2O	4.00	0.19	3.68	0.16	4.15	0.26	3.74	0.09	3.65	0.09
K_2O	2.74	0.12	3.21	0.14	3.53	0.09	2.75	0.06	4.06	0.12
P_2O_5	0.08	0.04	0.07	0.04	0.03	0.03	0.03	0.02	0.10	0.05
Cl	0.10	0.03	0.10	0.02	0.11	0.03	0.12	0.02	0.13	0.03
(n)	*22*		*36*		*23*		*22*		*17*	
ppm										
V	27.4	2.2	19.8	2.8	3.6	5.6	13.1	0.6	43.1	7.0
Rb	111.7	3.1	127.1	7.9	79.5	3.0	76.4	2.8	159.6	4.7
Sr	183	8.9	135	31.5	37.7	1.7	108.7	4.6	150.9	16.2
Y	26.9	1.0	23.9	1.8	25.5	1.7	29.9	0.7	29.2	1.0
Zr	175	4.9	201	13.1	60.6	3.7	203	3.6	255.3	6.3
Nb	9.3	0.2	9.4	0.7	6.8	0.2	5.1	0.1	9.5	0.3
Ba	474	9	524	24	633	57	591	11	606	15
La	23.8	0.6	24.3	1.5	13.3	0.9	16.0	0.3	24.1	0.8
Ce	51.5	2.0	49.8	3.2	29.4	2.0	36.7	0.9	54.0	2.1
Pr	5.6	0.2	5.2	0.4	3.3	0.2	4.4	0.2	6.1	0.3
Nd	22.3	1.2	20.5	1.6	13.4	1.3	19.2	0.7	24.3	1.1
Sm	4.7	0.5	4.3	0.5	3.3	0.3	4.8	0.5	5.3	0.4
Eu	1.09	0.12	0.81	0.08	0.45	0.12	0.75	0.06	0.83	0.07
Gd	4.6	0.6	3.7	0.5	3.2	0.3	4.6	0.2	4.6	0.3
Dy	4.5	0.3	4.0	0.3	3.9	0.3	5.0	0.2	4.8	0.3
Er	3.1	0.3	2.6	0.3	2.7	0.4	3.2	0.2	3.1	0.2
Yb	3.1	0.4	2.8	0.3	3.2	0.4	3.4	0.3	3.3	0.3
Lu	0.46	0.02	0.43	0.04	0.49	0.07	0.52	0.03	0.50	0.05
Hf	4.6	0.2	5.1	0.5	2.4	0.3	5.9	0.3	7.1	0.3
Ta	0.67	0.02	0.72	0.06	0.66	0.07	0.39	0.02	0.69	0.03
Pb	19.9	0.9	21.4	2.5	7.8	0.7	14.7	0.6	22.9	0.8
Th	9.3	0.5	10.5	1.1	4.3	0.5	6.2	0.2	13.6	0.7
U	2.4	0.2	2.6	0.3	2.0	0.1	1.9	0.1	3.4	0.1
(n)	*8*		*19*		*17*		*11*		*10*	

with the broadly homogeneous major element composition.

5.1.2. SG14-1554 (12,922 ± 58 IntCal20 yrs BP)

SG14-1554 is a relatively heterogeneous rhyolitic cryptotephra (74.3-6-77.0 wt% SiO_2 [$n = 34$]) which displays a largely medium-K (2.7–3.5 wt% K_2O) calc-alkaline affinity (Fig. 4A; Table 3). Using increasing SiO_2 content as a fractionation index CaO (2.0–1.3 wt%), Al_2O_3 (13.7–12.3 wt%) and FeOt (2.0–1.5 wt%) contents decrease, and K_2O increases, while Na_2O (4.1–3.4 wt%) and TiO_2 (0.5–0.3 wt%) contents are broadly constant. Consistent with the major elements, incompatible trace elements again show some heterogeneity (7.6–11.7 ppm Th; 163–221 ppm Zr; 18.9–26.3 ppm Y [$n = 19$]; Fig. 6) The glasses are enriched in Rb relative to the HFSE, with a strong depletion in Nb and Ta (Fig. 5), whilst also being enriched in LREE relative to the HREE where $La/Yb_N = 6.3 \pm 0.6$ (1σ; Fig. 5).

5.1.3. SG14-1579 (13,320 ± 64 IntCal20 yrs BP)

SG14-1579 is a homogeneous rhyolitic cryptotephra (78.0 ± 0.2 wt % SiO_2 [1σ; $n = 23$]) which straddles the boundary between a medium-K calc-alkaline and high-K calc-alkaline classification (3.5 ± 0.1 wt% K_2O; Fig. 4A; Table 3). No significant major element oxide variations are observed for this tephra (e.g., 0.6 ± 0.1 wt% FeOt and 0.6 ± 0.1 wt% CaO; Fig. 4). Consistent with major element compositions, the incompatible trace element content of the glasses are homogenous (4.3 ± 0.5 ppm Th; 6.8 ± 0.2 ppm Nb; 25.5 ± 1.7 ppm Y [$n = 17$]; Fig. 5). The glasses are enriched in Rb relative to the HFSE, with a strong depletion in Nb and Ta (Fig. 5). The glasses show low contents of Sr (37.7 ± 1.7 ppm) and Zr (60.6 ± 3.7 ppm), marked by noticeable depletions in the mantle normalised profile (Fig. 5). The glasses also show a relatively shallow REE profile relative to the overlying cryptotephra deposits, where $La/Yb_N = 3.0 \pm 0.3$ (1σ; Fig. 5).

5.1.4. SG14-1798 (16,619 ± 74 IntCal20 yrs BP)

SG14-1798 is a rhyolitic cryptotephra (78.0 ± 0.3 wt% SiO_2; $n = 22$), with a homogeneous major element composition (e.g., 1.3 ± 0.04 wt% CaO; 1.3 ± 0.05 wt% FeOt and 0.29 ± 0.03 wt% TiO_2; Fig. 4) and a clear calc-alkaline affinity (2.7 ± 0.1 wt% K_2O; Fig. 4A; Table 3). As with the major element compositions, the incompatible trace element content of the SG14-1798 glasses are homogenous (e.g., 6.2 ± 0.2 ppm Th, 203 ± 4 ppm Zr and 29.9 ± 0.7 ppm Y; [1σ] Fig. 6). The glasses are enriched in Rb relative to the HFSE, with strong depletions in Nb and Ta (Fig. 5). The glasses display a similarly shallow REE profile to the overlying cryptotephra deposits, where $La/Yb_N = 3.4 \pm 0.3$ (1σ; Fig. 5).

5.1.5. SG14-1806 (16,789 ± 72 IntCal20 yrs BP)

SG14-1806 is a heterogeneous rhyolitic cryptotephra (72.0–75.3 wt % SiO_2; $n = 17$) with a clear high-K calc-alkaline affinity (3.9–4.4 wt% K_2O; Fig. 4A; Table 3), although a dominant glass population resides at ~73 wt% SiO_2 and ~4.1 wt% K_2O. Overall, using increasing SiO_2 content as a fractionation index CaO (2.2–1.4 wt%), Al_2O_3 (14.2–13.0 wt%), TiO_2 (0.6–0.4 wt%) and FeOt (2.5–1.5 wt%) content decrease, while K_2O content clearly increases (Fig. 4A). Incompatible trace elements contents show some variability (e.g., 12.6–14.3 ppm Th, 9.0–9.7 ppm Nb, 26.8–30.8 ppm Y; Fig. 6). The mantle-normalised trace element

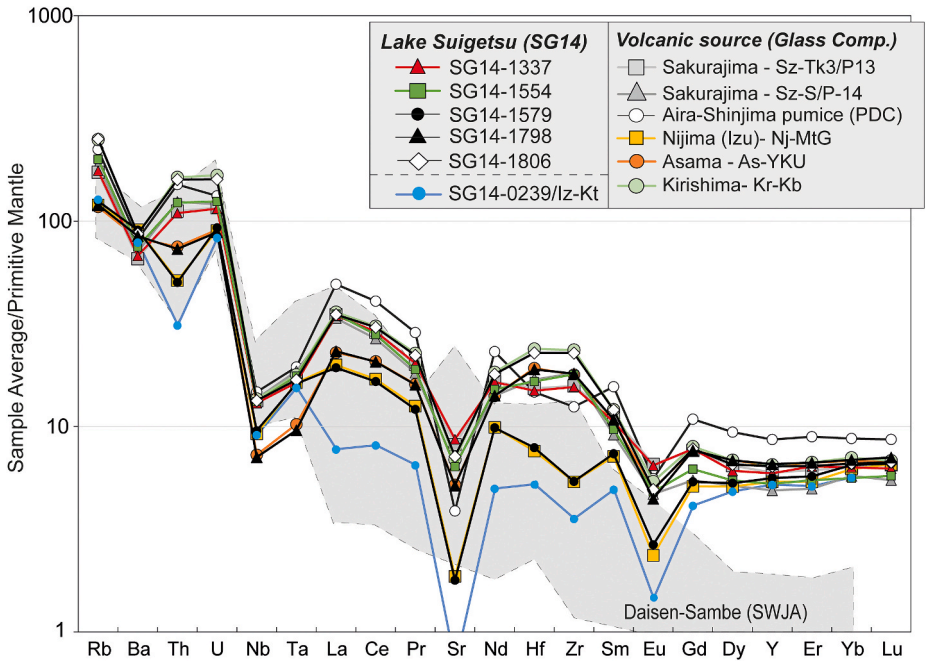


Fig. 5. Sample-averaged Primitive Mantle normalised trace element compositions of the five cryptotephra deposits identified within the early Holocene to Late-glacial sediments of Lake Suigetsu. These data are compared to new reference chemical datasets produced for chrono-stratigraphically relevant eruption units at Sakurajima (Aira caldera), Karakunidake (Kirishima), Asama and Niijima volcanoes. Primitive mantle values used for normalisation follow Sun and McDonough (1989). Envelope for the SWJA eruption deposits of Daisen and Sambe volcanoes is based on data presented in Albert et al. (2018). Also provided for comparative purposes is the trace element signature of the Late Holocene tephra SG14-0239, which is correlated to the Izu-Kōzushima-Tenjosan (Iz-Kt) tephra (McLean et al., 2018).

profile reveals the glasses are enriched in Rb relative to the HFSE, with strong depletions in Nb and Ta (Fig. 5). They also display relative enrichments in Hf and Zr, and clear LREE enrichment relative to the HREE, where $La/Yb_N = 5.3 \pm 0.4$ (1σ; Fig. 5).

6. Discussion

6.1. Establishing source regions for the SG14 cryptotephra

All five Lake Suigetsu cryptotephra analysed are rhyolitic (~72–78 wt% SiO_2) and show medium-K calc-alkaline to high-K calc-alkaline affinities (2.5–4.5 wt% K_2O; Fig. 4) suggesting they most likely derive from Japanese or Izu Arc volcanic sources and are inconsistent with nearby potassic intra-plate volcanoes. This is supported by the mantle-normalised trace element profiles of the volcanic glasses for each cryptotephra, revealing depletions in Nb and Ta indicative of subduction related volcanism (Fig. 5). We identify four distinct mantle-normalised profiles and levels of incompatible trace element enrichment in the five cryptotephra layers indicating potentially four different sources/regions (Fig. 5). Two of the cryptotephra layers have similar mantle normalised profiles SG14-1337 and SG14-1554 suggesting they are likely from the same source region or volcano (Fig. 5).

The K_2O content of the melt (glass) erupted at Japanese volcanoes varies depending on the particular arc they reside upon and their position relative to the subduction zone (e.g., forearc/rear-arc). Consequently, K_2O provides a useful first order means of discriminating the volcanic source area of distal tephra deposits like those preserved in Lake Suigetsu. The >2.5 wt% K_2O content of these rhyolitic cryptotephra layers mean a provenance from volcanoes along the northern North East Japan Arc (NEJA) and the Southern Kurile Arc is very unlikely, given these volcanoes generally erupt melt compositions with lower K_2O content based on reference volcanic glass datasets (e.g., Kimura et al., 2015; Albert et al., 2019, Fig. 4a). Similarly, the high K_2O content of these cryptotephra layers precludes the identification of ash fall from the largest Japanese Late-glacial eruption, the Towada Hachinohe (To-H, Fig. 4) dated at 15,615–15,895 IntCal20 yrs BP (Muscheler et al., 2020).

The K_2O content of SG14-1337, SG14-1554, SG14-1579 and SG14-1806 tephra deposits all reside on calc-alkaline (CA) and High-K calc-alkaline (HKCA) series trends which are consistent with magmas erupted at calderas within the Southern Volcanic and Central Kyushu volcanic regions. A correlation to the nearby Daisen and Sambe volcanoes which also erupt CA/HKCA tephra deposits is immediately precluded by the absence of strong depletions in the HREE (e.g., elevated La/Yb_N ratios) a feature of these SWJA volcanoes (Albert et al., 2018).

The thorium content of the volcanic glasses offers another important means of discriminating Japanese eruption sources. Evolved, rhyolitic products (>69 wt%), from Kyushu volcanoes are more enriched in Th (>7 ppm; Fig. 6) than other Japanese volcanic source regions (e.g., northern NEJA, <7 ppm). Consequently, the elevated Th content of SG14-1337, SG14-1554 and SG14-1806 glasses are consistent with a Kyushu source (Fig. 6). In contrast, SG14-1579 and SG14-1798 have a lower Th content (Fig. 6). In the case of SG14-1579 glasses, the flatter REE profile, a low Th content, combined with K_2O content more elevated than those erupted at NEJA sources, would point to a probable origin along the Izu Arc. The SG14-1798 cryptotephra has lower K_2O and Th content than rhyolitic Kyushu derived magmas and is broadly more consistent with the products erupted along the NEJA. However, the REE profile is relatively flat, similar to those seen in Izu arc products, which might suggest a volcanic source positioned at the conjunction of the NEJA and Izu arcs within central Honshu.

6.2. Constraining source eruptions: chronological, climato-stratigraphic and archaeological significance

In the section below we consider the five cryptotephra layers in the context of known early Holocene and Late-glacial eruptions at volcanic centres in southern Kyushu, central Honshu, and along the northern Izu

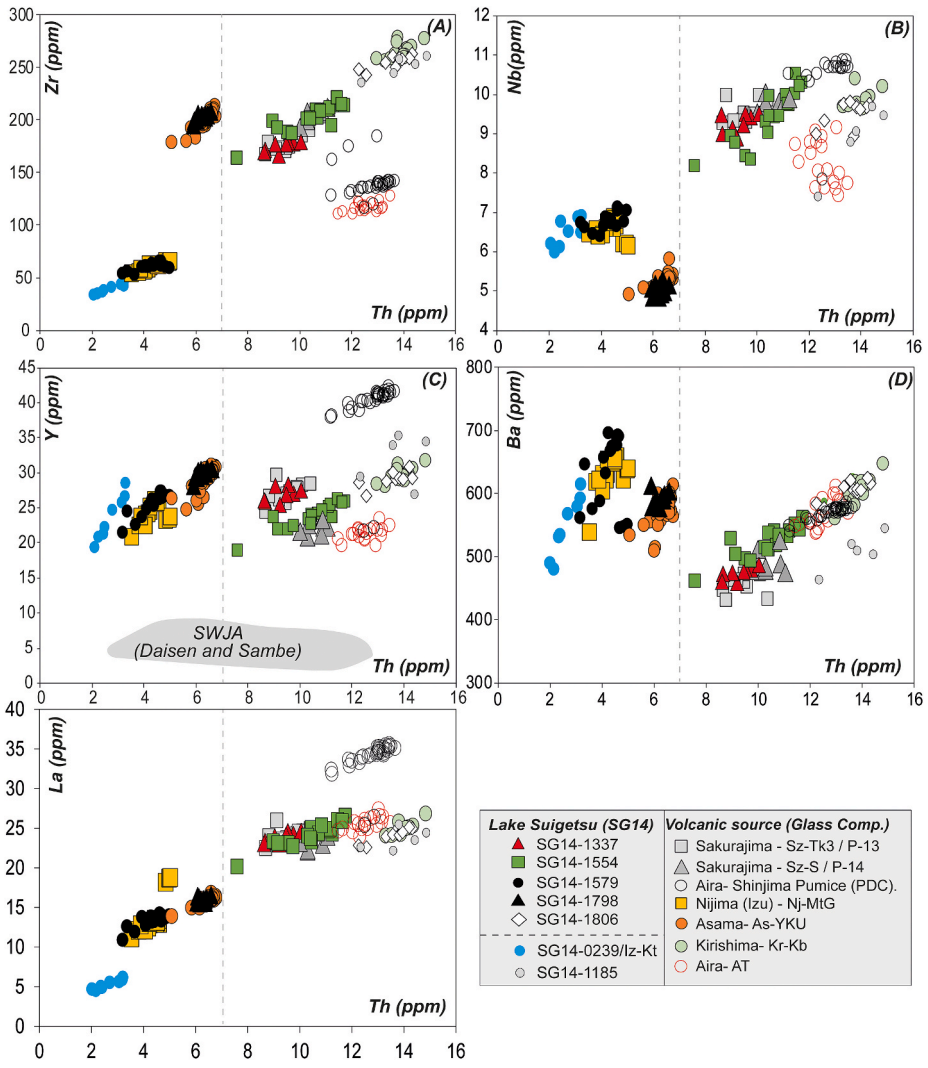


Fig. 6. Trace element compositions of individual volcanic glass shards from the five cryptotephra deposits identified within the early Holocene to Late-glacial sediments of Lake Suigetsu. These data are compared to new reference glass chemical datasets produced for chrono-stratigraphically relevant eruption units at Sakurajima (Aira caldera), Karakunidake (Kirishima), Asama and Niijima volcanoes (See text for more information). The dashed lined at 7 ppm Th content broadly delimits the rhyolitic (≥69 wt% SiO_2) products of northern NEJA/Southern Kurile Arc (<7 ppm) from those of the Kyushu volcanoes (>7 ppm) based on existing glass datasets available for widespread Japanese tephras (Kimura et al., 2015; Albert et al., 2019). Envelope for the SWJA eruption deposits of Daisen and Sambe volcanoes is based on Y data presented in Albert et al. (2018) and best illustrates their depletion in the HREE (Adakites). AT glass analyses are from Albert et al. (2019). Also provided for comparative purposes are the trace element glass compositions of the Late Holocene Lake Suigetsu tephra SG14-0239, which was correlated to the Izu-Kōzushima-Tenjosan (Iz-Kt) tephra, and SG14-1185 (McLean et al., 2018).

Arc which are considered ≥ M 4.0 or VEI 4 (Table 1). Correlations are established using new volcanic glass chemistry of near-source (Table 4; Supplementary Material 1) and distal (Table 5) reference samples and are supported by chrono-stratigraphic constraints. Whilst exploring the correlations we also discuss the chronological, palaeoclimatological and archaeological significance of the cryptotephra layers identified in the Lake Suigetsu sedimentary archive.

6.2.1. Sakurajima/Aira caldera (SG14-1337/Sz-Tk3 and SG14-1554/Sz-?)

Cryptotephra SG14-1337 is preserved in the early Holocene sediments of Lake Suigetsu (Fig. 7) and is dated using the site's high-precision chronology to 10,623 ± 50 IntCal20 yrs BP (2σ). Its medium-K CA affinity is consistent with the products of the Kyushu SVZ, and specifically the rhyolitic products of Sakurajima (Sz) volcano positioned on the southern edge of the Aira caldera. The major and trace element glass compositions of SG14-1337 are indistinguishable from those of the rhyolitic Plinian/sub-Plinian fall deposits associated with the early Holocene Takatoge 3 (Sz-Tk3) or Pumice 13 eruption (Figs. 4–6). We recalibrate the radiocarbon age of charcoal imbedded within the deposit of 9540 ± 90 ^{14}C yrs BP (Okuno et al. (1997) to 10,585–11,175 IntCal20 yrs BP (2σ), which is in very good agreement with the Lake Suigetsu derived age (10,623 ± 50 IntCal20 yrs BP; Fig. 8). Isopach maps for the Sz-Tk3 tephra show a predominantly easterly dispersal for the fall deposits of the eruption which has an estimated tephra volume of 1.3 km^3 (Okuno et al., 1999; Kobayshi and Tameike, 2002). The discovery of Sz-Tk3 at Lake Suigetsu, 650 km north-east of Sakurajima, extends the known distribution of ash fall associated with this eruption and highlights the potential to recognise it in other sites north of the volcano. This is the second largest eruption in the time-interval of study and the precise age presented here is important for refining the chronology of Jomon archaeological sites in southern Kyushu (Fig. 7). For instance, around Kagoshima Bay and Sakurajima volcano the Sz-Tk3 tephra is found in excavation levels associated with the Earliest Jomon housing settlements (e.g., Uenohara), and which clearly mark an increase in permanent housing indicative of early

Table 4
Average major and trace element glass compositions of Late-glacial to early Holocene near-source eruption deposits analysed here for direct comparison with the Lake Suigetsu cryptotephra deposits. Major element glass data has been normalised (water-free). Full geochemical datasets are available in the Supplementary Material 1.

Tephra	Sz-Tk3 (P-13)		Sz-S (P-14)		Sz-S (P-14)		A-Shinjima Ign.		Nj-MtG		Kr-Kb	
Deposit	Pumice fall		Pumice fall		Pumice fall		PDC		Pumice fall		Pumice fall	
Location	Takatoge Pass		Takatoge Pass		Ushinesakai		Moeshima Island		Niijima Island		Takaharu	
wt.%	Ave.	1σ	Ave.	1σ	Ave.	1σ	Ave.	1σ	Ave.	1σ	Ave.	1σ
SiO_2	72.65	0.35	74.56	0.51	74.56	0.18	77.03	0.32	78.02	0.15	72.77	1.03
TiO_2	0.47	0.03	0.38	0.03	0.38	0.03	0.10	0.03	0.08	0.02	0.51	0.04
Al_2O_3	14.33	0.20	13.69	0.37	13.60	0.12	12.83	0.16	12.72	0.10	14.08	0.76
FeOt	2.41	0.12	1.88	0.10	1.90	0.06	1.55	0.14	0.65	0.05	2.20	0.10
MnO	0.10	0.02	0.06	0.02	0.06	0.03	0.05	0.02	0.07	0.02	0.06	0.02
MgO	0.56	0.07	0.44	0.04	0.44	0.03	0.06	0.03	0.09	0.02	0.49	0.03
CaO	2.42	0.11	2.04	0.12	2.08	0.03	1.21	0.08	0.56	0.04	2.14	0.58
Na_2O	4.09	0.10	3.76	0.13	3.89	0.08	3.84	0.12	4.07	0.13	3.45	0.13
K_2O	2.81	0.07	3.01	0.05	2.91	0.04	3.21	0.10	3.61	0.12	4.08	0.21
P_2O_5	0.09	0.03	0.07	0.04	0.06	0.04	0.02	0.03	0.02	0.02	0.09	0.03
Cl	0.08	0.02	0.11	0.02	0.10	0.01	0.09	0.01	0.10	0.02	0.13	0.02
(n)	*11*		*51*		*23*		*69*		*41*		*27*	
ppm												
V	27.3	2.0	26.8	1.5	25.0	0.9	<LOD	<LOD	1.6	0.9	44.3	6.8
Rb	110	3.1	120	2.3	118	3.5	142	2.1	76.1	3.2	159	3.7
Sr	173	12.4	138	6.1	146.3	5.0	81.9	7.9	39.4	7.3	146	8.3
Y	27.2	1.4	22.2	0.8	24.4	0.9	39.3	4.8	24.5	1.5	29.7	1.0
Zr	176	7.1	204	6.4	206	5.9	140	13.1	60.3	3.2	264	7.3
Nb	9.5	0.3	9.8	0.2	9.6	0.3	10.5	0.7	6.6	0.2	9.7	0.3
Ba	458	16.3	497	19.6	565	39.2	570	10.4	635	27.9	605	21
La	24.1	1.0	23.1	0.9	24.6	1.0	33.9	2.3	13.7	2.2	24.8	0.8
Ce	51.2	2.4	47.5	1.7	48.2	1.8	72.4	5.8	30.2	3.9	54.7	2.3
Pr	5.6	0.3	5.0	0.2	5.3	0.2	7.9	0.7	3.5	0.4	6.3	0.3
Nd	22.4	1.3	19.1	0.9	20.4	0.6	31.4	3.3	13.4	1.7	24.9	1.0
Sm	4.94	0.34	4.05	0.37	*4.33*	*0.25*	6.94	0.87	3.18	0.32	5.37	0.31
Eu	1.10	0.10	0.79	0.07	0.85	0.09	0.94	0.11	0.40	0.04	0.91	0.08
Gd	4.56	0.48	3.27	0.32	3.86	0.18	6.47	0.83	3.05	0.24	4.76	0.25
Dy	4.76	0.38	3.80	0.29	4.22	0.23	6.93	0.89	3.76	0.29	5.06	0.24
Er	2.94	0.20	2.39	0.23	2.57	0.16	4.28	0.55	2.59	0.26	3.21	0.23
Yb	3.11	0.22	2.83	0.18	2.86	0.23	4.31	0.50	3.06	0.25	3.48	0.22
Lu	0.48	0.03	0.41	0.05	0.44	0.05	0.64	0.07	0.49	0.04	0.51	0.04
Hf	4.7	0.2	5.2	0.2	5.4	0.1	4.6	0.4	2.3	0.2	7.4	0.4
Ta	0.72	0.04	0.76	0.04	0.78	0.04	0.80	0.04	0.67	0.03	0.73	0.03
Pb	21.5	1.6	21.3	0.6	20.9	0.9	24.6	1.3	7.8	0.8	23.5	1.2
Th	9.5	0.5	10.6	0.4	11.0	0.3	12.8	0.6	4.4	0.4	13.9	0.4
U	2.4	0.1	2.5	0.2	2.7	0.1	2.8	0.1	1.9	0.1	3.5	0.2
(n)	*11*		*7*		*7*		*31*		*20*		*15*	

Tephra	As-YP		As- Upper Glass PDC		As-Komoro PDC		As–K		As–K	
Deposit	Pumice fall		PDC		PDC		Pumice fall		Pumice fall	
Location	Kojin		Kojin		Tsumagoi		Tsumagoi		Kitakaruizawa	
wt.%	Ave.	1σ	Ave.	1σ	Ave.	1σ	Ave.	1σ	Ave.	1σ
SiO_2	77.38	0.16	77.62	0.19	77.61	0.21	77.73	0.18	77.79	0.35
TiO_2	0.30	0.03	0.29	0.03	0.30	0.03	0.30	0.03	0.30	0.03
Al_2O_3	12.27	0.13	12.18	0.14	12.25	0.10	12.16	0.11	12.13	0.19
FeOt	1.47	0.12	1.42	0.08	1.43	0.06	1.39	0.05	1.38	0.08
MnO	0.04	0.02	0.04	0.02	0.05	0.02	0.05	0.02	0.05	0.02
MgO	0.27	0.03	0.24	0.03	0.26	0.03	0.26	0.04	0.23	0.03
CaO	1.41	0.03	1.31	0.04	1.39	0.03	1.33	0.04	1.30	0.10
Na_2O	3.99	0.15	3.95	0.12	3.76	0.12	3.94	0.10	3.93	0.06
K_2O	2.67	0.08	2.81	0.04	2.75	0.05	2.66	0.06	2.71	0.08
P_2O_5	0.03	0.03	0.02	0.02	0.03	0.02	0.03	0.03	0.03	0.02
Cl	0.16	0.02	0.12	0.02	0.16	0.02	0.16	0.02	0.15	0.02
(n)	*41*		*75*		*38*		*49*		*23*	
ppm										
V	15.3	0.8	14.4	2.5	14.6	0.5	13.7	1.0	14.2	0.9
Rb	72.5	2.4	74.8	1.6	74.1	2.1	72.2	1.4	72.2	2.4
Sr	118	2.6	109	4.2	117	3.1	109	3.4	112	7.7
Y	30.3	0.9	29.4	1.4	30.1	0.6	29.7	0.8	29.8	1.0
Zr	208	6.1	201	7.9	205	3.9	200	5.2	199	7.6
Nb	5.3	0.2	5.2	0.1	5.2	0.1	5.1	0.1	5.2	0.2
Ba	576	16.2	579	22	595	7.6	570	17.9	576	30.7
La	16.0	0.3	15.8	0.7	16.1	0.3	15.8	0.5	15.7	0.6
Ce	37.5	1.8	36.8	1.5	37.8	0.7	36.8	1.2	36.4	1.1
Pr	4.6	0.2	4.4	0.2	4.5	0.2	4.5	0.1	4.4	0.2
Nd	20.1	0.9	19.1	0.9	19.6	0.5	19.4	0.8	19.3	0.8
Sm	5.1	0.5	4.7	0.3	4.9	0.3	4.7	0.3	4.8	0.4

(*continued on next page*)

Table 4 (*continued*)

Tephra	As-YP		As- Upper Glass PDC		As-Komoro PDC		As–K		As–K	
Deposit	Pumice fall		PDC		PDC		Pumice fall		Pumice fall	
Location	Kojin		Kojin		Tsumagoi		Tsumagoi		Kitakaruizawa	
wt.%	Ave.	1σ	Ave.	1σ	Ave.	1σ	Ave.	1σ	Ave.	1σ
Eu	0.84	0.11	0.84	0.33	0.82	0.06	0.79	0.05	0.79	0.06
Gd	4.8	0.3	4.6	0.3	4.4	0.4	4.5	0.3	4.6	0.2
Dy	5.2	0.3	5.1	0.3	5.1	0.2	5.1	0.2	5.1	0.3
Er	3.3	0.2	3.2	0.2	3.3	0.2	3.3	0.2	3.3	0.3
Yb	3.5	0.3	3.4	0.4	3.4	0.2	3.4	0.2	3.5	0.2
Lu	0.54	0.04	0.50	0.04	0.51	0.03	0.51	0.03	0.52	0.03
Hf	6.2	0.3	6.0	0.4	6.1	0.3	5.9	0.3	5.9	0.3
Ta	0.43	0.03	0.42	0.02	0.41	0.02	0.41	0.02	0.41	0.02
Pb	14.5	0.9	15.0	1.2	14.2	0.8	14.3	0.5	14.3	0.7
Th	6.5	0.3	6.4	0.3	6.5	0.3	6.4	0.3	6.4	0.2
U	1.9	0.1	1.9	0.1	2.0	0.1	1.9	0.1	1.9	0.2
(n)	*21*		*44*		*35*		*15*		*19*	

Table 5
Average major and trace element glass compositions of proposed distal Asama-Y/K/U equivalents analysed for direct comparison with the Lake Suigetsu cryptotephra SG14-1798. Major element glass data has been normalised (water-free). Full geochemical datasets are available in Supplementary Material 1. References relate to the reported occurrence of the Asama tephra (a) Nagahashi et al., 2022; (b) Nakajima et al. (1996); (c) Okuno et al. (2011); (d) This study.

Tephra	As–K [a]		As–K [b]		As–K [c]		As-YKU [d]	
Core	YK10-07 - PC09		GH892-22		IMG06		AOK-1	
Depth (cm)	428.7–428.8		303.0–303.2		1217.7–1218.0		52.5–53.0	
wt.%	Ave.	±1σ	Ave.	±1σ	Ave.	±1σ	Ave.	±1σ
SiO_2	77.54	0.14	77.54	0.11	77.78	0.19	77.81	0.26
TiO_2	0.31	0.03	0.31	0.03	0.30	0.04	0.30	0.01
Al_2O_3	12.34	0.11	12.30	0.10	11.97	0.07	12.25	0.21
FeO	1.43	0.05	1.44	0.06	1.44	0.09	1.39	0.08
MnO	0.05	0.02	0.04	0.02	0.04	0.03	0.05	0.01
MgO	0.25	0.03	0.26	0.02	0.26	0.02	0.22	0.04
CaO	1.32	0.04	1.33	0.03	1.34	0.05	1.30	0.10
Na_2O	3.90	0.13	3.90	0.09	3.88	0.09	3.65	0.36
K_2O	2.68	0.05	2.68	0.04	2.81	0.08	2.89	0.15
P_2O_5	0.04	0.03	0.04	0.03	0.03	0.02	0.04	0.02
Cl	0.15	0.02	0.15	0.03	0.15	0.01	0.11	0.03
(n)	*24*		*23*		*17*		*7*	
ppm								
V	14.5	0.5	16.4	5.6	13.7	1.0	14.1	1.2
Rb	73.8	3.1	73.5	1.6	75.3	1.0	77.9	6.2
Sr	113	2.7	112.6	2.8	113	3.8	110.8	4.7
Y	29.4	0.9	29.6	0.6	30.1	0.4	30.1	0.6
Zr	198	6.9	200	4.9	202	2.8	201	3.9
Nb	5.1	0.1	5.1	0.2	5.1	0.0	5.2	0.1
Ba	587	9.8	585	13.8	591	9.3	595	12.1
La	15.5	0.4	15.7	0.4	16.2	0.3	16.1	0.4
Ce	35.7	1.2	36.4	1.3	37.3	0.6	37.6	0.9
Pr	4.4	0.2	4.4	0.2	4.6	0.1	4.5	0.1
Nd	19.0	0.7	18.9	0.8	19.8	0.5	19.5	0.7
Sm	4.6	0.3	4.9	0.4	4.8	0.2	4.8	0.3
Eu	0.75	0.04	0.81	0.08	0.78	0.04	0.79	0.06
Gd	4.5	0.4	4.6	0.5	4.5	0.2	4.5	0.3
Dy	4.9	0.3	5.3	0.4	5.1	0.3	5.2	0.3
Er	3.2	0.2	3.2	0.1	3.3	0.2	3.3	0.1
Yb	3.4	0.3	3.5	0.2	3.3	0.1	3.5	0.2
Lu	0.50	0.04	0.49	0.04	0.51	0.02	0.52	0.03
Hf	5.6	0.5	5.8	0.5	5.9	0.3	6.0	0.2
Ta	0.40	0.02	0.40	0.02	0.41	0.02	0.41	0.01
Pb	14.3	0.6	14.4	0.4	14.8	0.3	14.6	0.6
Th	6.3	0.4	6.2	0.5	6.4	0.2	6.4	0.2
U	1.9	0.1	2.0	0.1	1.9	0.1	1.9	0.1
(n)	*13*		*12*		*11*		*16*	

sedentism in Japan (Kurokawa, 2002; Pearson, 2006).

The glass compositions and in particular the trace element signature of SG14-1554 (217 cm below SG14-1337/Sz-Tk3) is similar to the rhyolitic products erupted at Sakurajima volcano, and Aira caldera more generally (Figs. 5 and 6). In the reported tephrostratigraphy from in and around the Aira caldera, and immediately below the Sz-Tk3 tephra, the most widely traced eruption unit relates to the Plinian pumice fall of the Sakurajima-Satsuma (Sz-S) which is dated to between 13,760–12,730 IntCal20 yrs BP based on radiocarbon dating of charcoals within the deposits, or the underlying palaeosols (Okuno et al., 1997, Fig. 8). Directly below the Sz-S are the PDC deposits known as the Shinjima (or Moeshima) pumice outcropping on Moeshima Island (within Aira caldera). They are believed to have derived from sub-marine activity at the small Wakamiko caldera within the eastern sector of the larger submerged caldera, with this eruption given an age of ~13 ka based on its stratigraphic position below the Sz-S (Moriwaki et al., 2017; Geshi et al., 2020). There is also another known Aira eruption unit, slightly older than the Shinjima pumice, the Takano base surge (A-Tkn), with this deposit first identified in the Fukaminato area (Moriwaki et al., 2017). A potential correlative of the A-Tkn is identified below the Shinjima PDC deposits within a Moeshima Island borehole (-290.5 m). The A-Tkn is loosely ascribed an age of ~19 ka based on it chrono-stratigraphic position (Moriwaki et al., 2017).

Comparison between the SG14-1554 major element compositions and those of near-source proximal fall deposits from the Sz-S collected to the east of Sakurajima reveal only minor chemical overlap. The majority of the cryptotephra analyses ($n = 34$) display glass compositions that extend to noticeably higher SiO_2 and K_2O, whilst lower CaO and Al_2O_3 content than the Sz-S glasses make a correlation based on these data difficult (Fig. 4). However, there is considerable trace element overlap between the SG14-1554 and Sz-S glasses (Fig. 6).

SG14-1554 and the Shinjima PDC deposits show some compositional overlap in most major elements, however there is clear evidence to exclude a correlation to this Aira caldera activity. SG14-1554 glasses, like those of Sakurajima, retain higher TiO_2 content (0.37 ± 0.4 wt%) than those of the Aira caldera including the Shinjima PDC unit (0.10 wt %), which are instead more akin to the older AT glass compositions, and those of the Aira Takano Base surge and potential correlatives (Fig. 4D). The lower TiO_2 content in the Aira caldera derived glasses are consistent with the fractionation of ilmenite, a phase observed in the AT products. Furthermore, major offsets are observed between the trace element contents of SG14-1554 and the Shinjima PDC deposits, for instance the Shinjima glass is more depleted in Zr and more enriched in REE contents relative to those of SG14-1554 (Figs. 5 and 6). Based on the available chemical data the most likely source of SG14-1554 remains Sakurajima volcano, however, a precise chemical correlation to an eruption unit remains illusive.

SG14-1554 is dated at 12,922 ± 58 IntCal20 yrs BP (2σ) in Lake

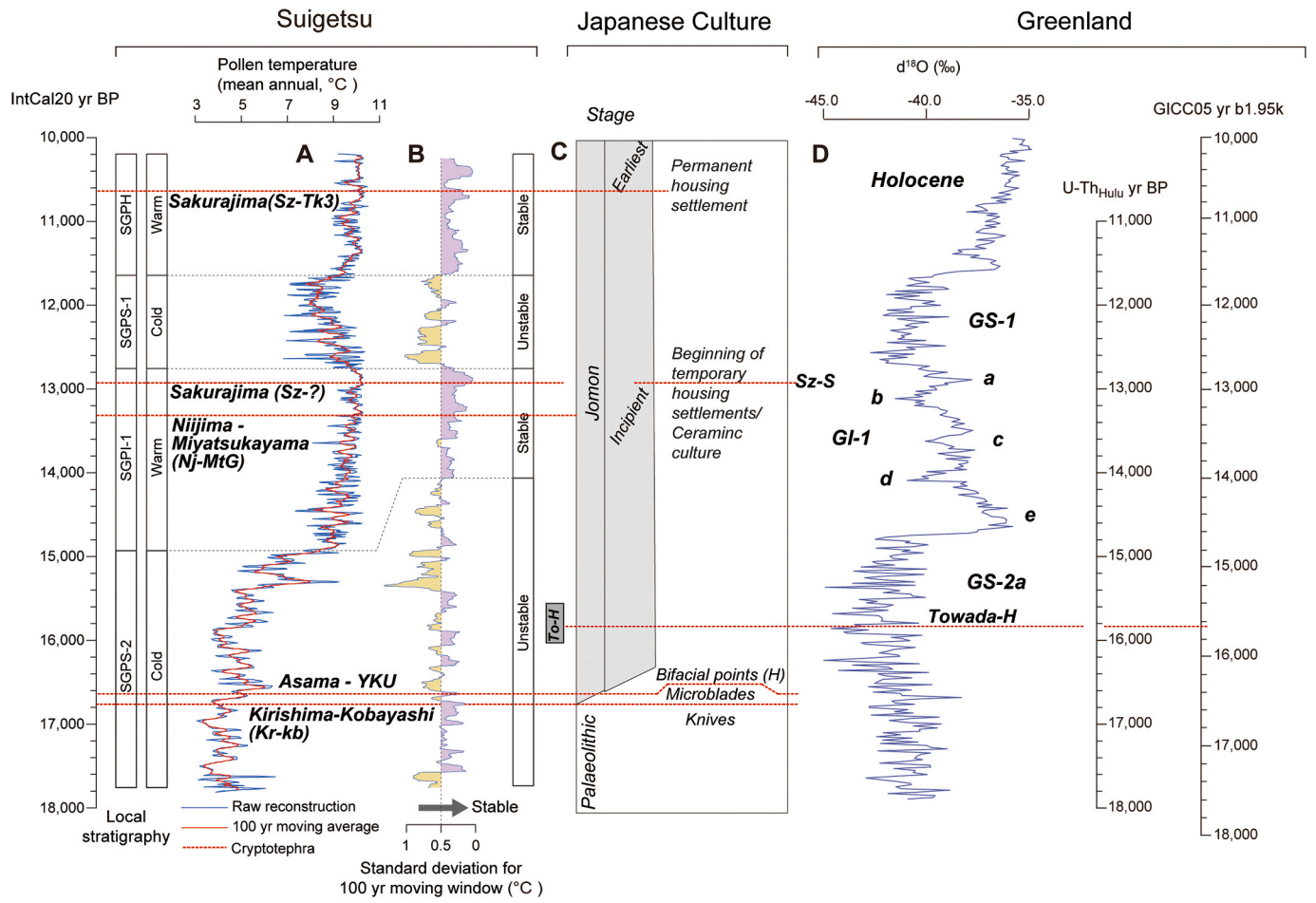


Fig. 7. A: SG14 cryptotephra layers plotted against the Lake Suigetsu pollen based mean annual temperature reconstruction spanning the Late-glacial to early Holocene (Nakagawa et al., 2021). Red line: 100 year moving average. Also shown are the local Suigetsu Pollen (SGP) event stratigraphy marking the boundaries between Stadial (S) and Interstadial (I) conditions and the onset of the Holocene (H) (Nakagawa et al., 2021) **B**: Reconstructed climate stability, standard deviation of the reconstructed temperature in 100 year moving window. The horizontal axis is inverted, i.e. the purple colour on the right-hand side indicates that the climate was stable during the century. **C.** Shows the newly dated SG14 cryptotephra integrated within cultural (archaeological) change in southern Japan (or central Japan in the case of (H; Honshu) associated with the transition from the Palaeolithic to Jomon period and early sedentism (adapted from Moriwaki et al., 2016). **D**: Places A-C in the context of rapid and typically greater amplitude climate variability captured by the Greenland ice cores d^{18}O (‰) record (NGRIP; Steffensen et al., 2008). The absolute age scale of the Greenland ice cores, GICC05 traditionally uses 2000 CE as the datum 'b2k'. Here to better facilitate comparisons to the IntCal20 chronology of Lake Suigetsu, we adopt a 1950 CE datum, instead expressing GICC05 as 'b1.95k', following Nakagawa et al. (2021). Furthermore, to aid reliable comparison between Lake Suigetsu (IntCal20) pollen temperature reconstruction and the Greenland d^{18}O (‰) record, the latter is also presented against the U-Th$_{Hulu}$ timescale (11,000–18,000 U-Th$_{Hulu}$ yr BP) following the transfer function of Adolphi et al. (2018). The timing of the To-H eruption reported as a cryptotephra isochron in the Greenland ice cores at 15,706 ± 226 yrs b2k (Bourne et al., 2016), is expressed here using a 1950 datum as 15,656 ± 226 yrs b1.95k.

Suigetsu and provides a critical isochron positioned at the end of the Late-glacial Interstadial, and immediately prior to the return to colder stadial conditions in Japan (Suigetsu Pollen Stadial [SGPS] −1), this being broadly equivalent to the North-west European Younger Dryas cooling event, and to Greenland Stadial 1 (GS-1; Fig. 7). Interestingly, the age of this cryptotephra is consistent with the near-source dating of the M 5.9 Plinian Sz-S eruption (Fig. 8). Similarly, the climato-stratigraphic position of SG14-1554 at Lake Suigetsu, is consistent with the Sz-S tephra which is also found just prior to the onset of Stadial (Younger Dryas) conditions as reconstructed from sediments in a north-east China Sea core (Moriwaki et al., 2016). Therefore, despite the chemical offsets, given the consistency in age and climato-stratigraphic position of SG14-1554 and the Sz-S tephra, a potential link cannot be entirely ruled out. One possibility is that the near-vent reference deposits sampled here at two locations to the east of Sakurajima, are not fully representative of the full compositional variability of the eruption. Our analyses focus on the Plinian fall deposits, so potentially analyses of any associated PDC deposits might offer better overlap with SG14-1554. An alternative scenario is that SG14-1554 relates to a separate eruption of Sakurajima that is closely-spaced in time and that has not yet been recognised in near-source exposures or other distal records, although this is unlikely as there is a well-established near-source tephrostratigraphy for the volcano (Okuno et al., 1997).

Certainly, if future near-source investigations of Sz-S deposits were able to demonstrate an unequivocal geochemical link between the SG14-1554 and the Sz-S eruption this would be extremely significant from a palaeoclimatological point of view. Its stratigraphic position immediately prior to the onset of an abrupt cooling event makes it an important marker for assessing spatial leads and lags in the climate system at this important transition. Indeed, the Sz-S has been recently traced over 2000 km south-west of Sakurajima to the Huguangyan Maar lake record in southern China (Fig. 4; Sun et al., 2021), offering the tantalising opportunity to synchronise extremely disparate Asian palaeoclimate archives. Verifying the correlation between Sz-S and SG14-1554 would also provide further Lake Suigetsu derived chronological constraints on the earliest Early Jomon archaeological sites.

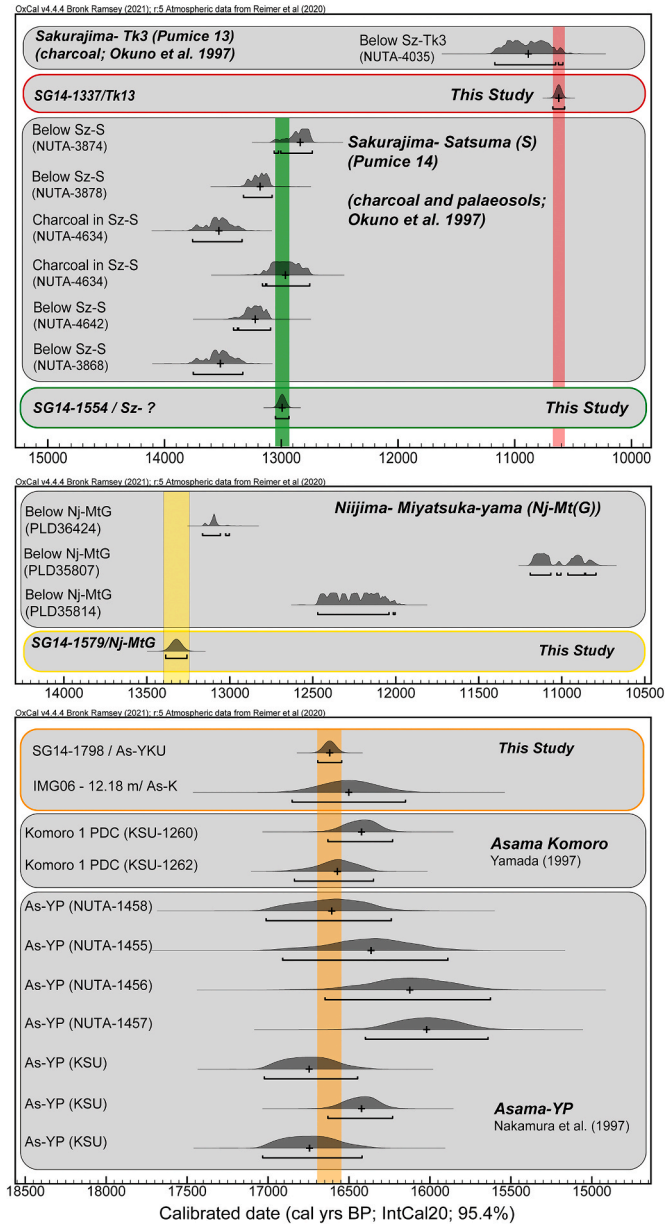


Fig. 8. Lake Suigetsu modelled age estimates (95.4% confidence) of SG14 cryptotephra layers compared to near-source radiocarbon dating buried tree-stumps, charcoals and palaeosols associated with probable source eruption units. All proximal dating has been re-calibrated using the IntCal20 calibration curve to enable direct comparison with the SG14 IntCal20 ages. See text for discussion of the ages and the source references.

6.2.2. Niijima Island (SG14-1579/Nj-MtG)

SG14-1579 dated at 13,320 ± 64 IntCal20 yrs BP (2σ) is positioned within the Late-glacial Interstadial sediments of Lake Suigetsu (Suigetsu Pollen Interstadial 2; SGPI2), which coincide with Greenland Interstadial 1 (Fig. 7). A combination of a relatively high K_2O content (3.5 ± 0.1 wt%), low Th content (4.3 ± 0.5 ppm) and a relatively flat REE profile ($La/Yb_N = 3.0 \pm 0.3$) points to a probable source along the Izu arc. The incompatible trace element contents of SG14-1579 glass shards are also similar to a late Holocene tephra, SG14-0239 (Fig. 6), which has been firmly correlated to the 838 CE eruption of Kozushima island along the north Izu arc (McLean et al., 2018). This similarity in certain incompatible elements content between SG14-1579 and Izu-Kozushima-Tenjosan (Iz-Kt)/SG14-0239 tephra reinforces the idea of a volcanic source region in the northern Izu arc (Fig. 6).

Chrono-stratigraphically relevant activity is reported on the neighbouring island of Niijima (20 km north of Kozushima) relating to the Niijima Miyatsuka-yama Group (Nj-MtG) eruptive succession (Kobayashi et al., 2020). Major and trace element glass compositions of SG14-1579 are consistent with the reference pumice fall deposits of the Niijima Miyatsuka-yama (Figs. 4–6). Proximal dating of these sub-Plinian/Plinian deposits is variable, with ^{14}C ages spanning a calibrated age range of 10,700–13,200 IntCal20 yrs BP (Fig. 8; Kobayashi et al., 2020), the imprecise nature of two of these ages may in part relate to their coincidence with plateaus in the radiocarbon calibration curve, or alternatively it could indicate that there were two or more closely spaced eruptions. The oldest of these ^{14}C age determinations broadly agrees with the SG14-1579 Lake Suigetsu modelled age of 13,320 ± 64 IntCal20 yrs BP (2σ; Fig. 8). This chronological agreement combined with its chemical similarity between the Niijima Miyatsuka-yama eruption deposits allows us to place more precise age constraints on the start of this eruptive episode on Niijima. The discovery of ash from a Niijima eruption deposited in Lake Suigetsu reinforces the fact that these islands south of Tokyo pose a significant ash fall risk to incredibly populated regions in central Japan.

6.2.3. Asama (SG14-1798/As-YKU)

The SG14-1798 glass shard compositions are consistent with the eruptive products of Late-glacial activity at Asama volcano in central Japan (Figs. 4–6). Specifically, the chemistry corresponds to a complex succession of Plinian fall and PDC units collectively referred to as the As-YKU tephra which are associated with a widespread ash dispersal traced across central and northern Honshu (Fig. 9A).

Here we compare the glass analysis of SG14-1798 directly to the major and trace element glass analysis of near-source samples from the main eruption units of the Asama-YKU. Sampling was conducted at three locations, Kojin (30 km) to the east of Asama, and Tsumagoi (11 km) and Kitakaruizawa (9 km) to the north-east (Fig. 9A). Kojin preserves the initial Plinian As-YP pumice fall unit, that is overlain by a well-sorted ash bed (Fig. 9B), which is interpreted here as ash fall, possibly relating to a co-PDC plume. This ash bed is labelled here as the As-Upper Glass (As-UG). At Tsumagoi a > 1 m thick poorly sorted PDC deposit known as the Komoro pumice flow deposit was identified, capped by the second Plinian fall deposit, As–K (Fig. 9D). The As–K pumice fall bed was also sampled nearby at Kitakaruizawa (Fig. 9C). Full descriptions of the deposits are reported in the Supplementary Material 2.

SG14-1798 glasses are clearly offset to higher SiO_2, lower CaO (Fig. 10A), FeOt and Sr (Fig. 10B) content relative to the initial Plinian fall deposits, As-YP. We therefore suggest that the distal cryptotephra at Lake Suigetsu is unrelated to the initial Plinian phase As-YP, which is dispersed toward the south and east of vent (Fig. 9A). The Komoro PDC deposits that were sampled from directly underlying the second Plinian phase, As–K, to the north-east of vent at Tsumagoi, are compositionally more consistent with the initial Plinian fall phase (As-YP), and again show very limited (CaO, FeOt and Sr) overlap with SG14-1798 (Fig. 10A and B). Given their chemical similarity (high-Ca, high-Sr), it would seem probable that the Komoro PDC deposits relate to the collapse of the initial (As-YP) Plinian column.

The SG14-1798 glass compositions are instead compatible with the subtly more evolved products of the second Plinian phase, the As–K fall. The glasses within the As–K pumice fall deposits sampled at both Tsumagoi and Kitakaruizawa, NE of vent, extend to lower CaO and Sr, very consistent with the SG14-1798 glass shards (Fig. 10A and B), and of all the near-vent units analysed arguably offers the best chemical agreement. Similarly, the glass compositions of the ash dominated, pumice poor, As-UG deposits stratigraphically positioned above the As-YP at Kojin east of Asama are also more evolved than the underlying As-YP pumice fall, and the Komoro PDC deposits (Fig. 9B and C). The relative stratigraphy relationship of the Kojin As-UG deposit and the second Plinian fall deposit, As–K, is unknown, however, from their consistent glass chemistries it is likely they were emplaced in the later phase of the

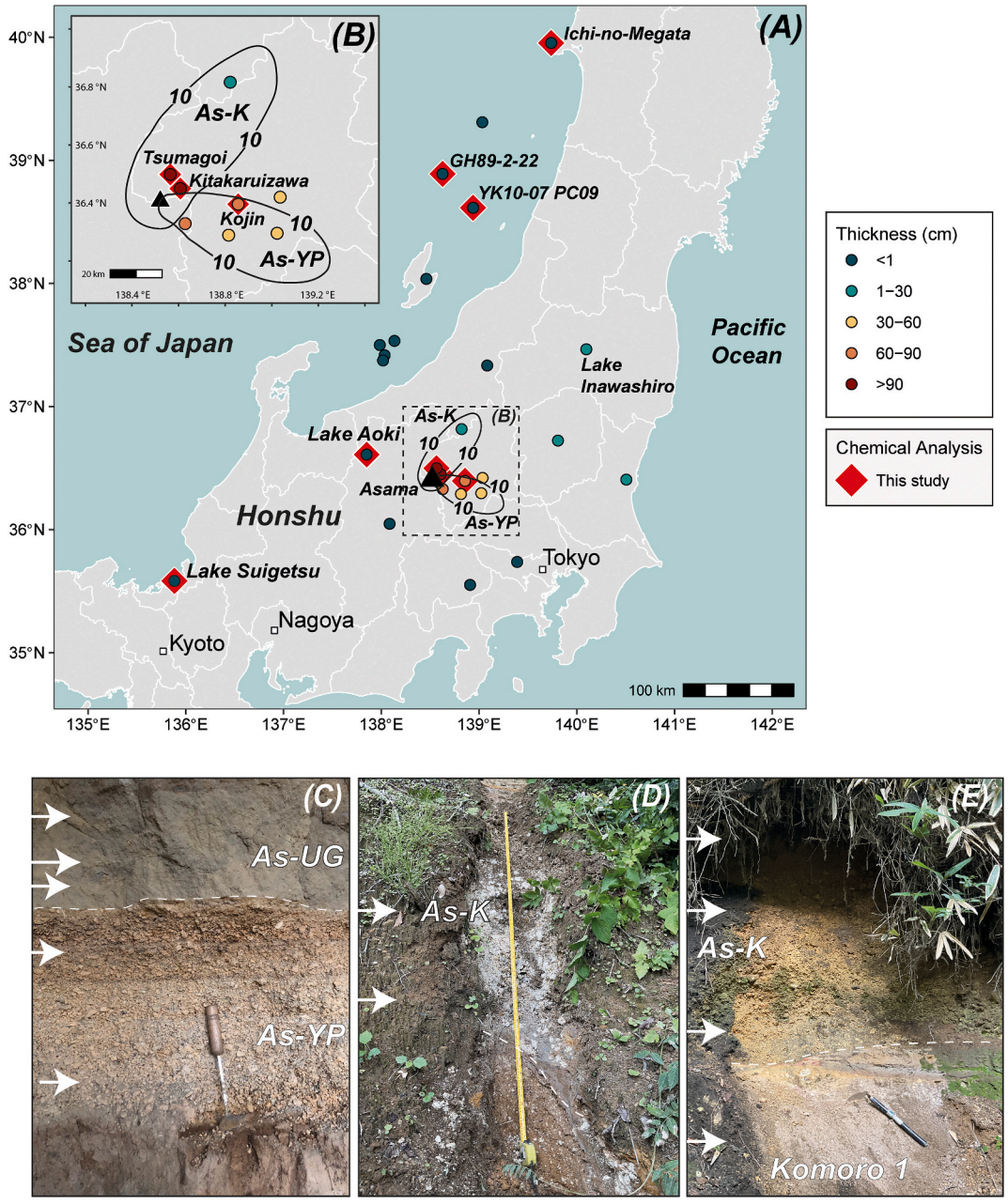


Fig. 9. A. Map of Honshu island, Japan, showing reported occurrences of tephra deposits associated with the Late-glacial Asama-YKU eruptive succession, including newly reported occurrences at Lake Suigetsu (SG14-1798) and Lake Aoki (AOK-15-1-53), both of which greatly extend the distribution of ash fall associated with this activity at Asama volcano. The 10 cm isopach are associated with the two Plinian fall phases As-YP and As–K and these are based on those presented in Machida and Arai (2003) and digitised in Uesawa et al. (2022). Deposit thicknesses represent the entire Asama-YKU succession present at a given site. **B:** inset show the sampling localities of the near-source deposit shown in C-E. Distal occurrences collated are reported in: Anma et al. (1990); Suzuki (1990); Suzuki, M (1991); Suzuki (1993); Tsuji (1996); Takemoto (1996); Nakajima et al. (1996); Kariya et al. (1998); Kuninaka (1999); Choi et al. (2002); Noshiro et al. (2004); Tsuji et al., 2004; Yoshida and Sugai (2005); Okuno et al. (2011); Nakamura et al. (2013); Hirose et al. (2014); Aoki (2020); Nagahashi et al.,.; **C:** Kojin As-YP pumice fall, capped by As-UG ash bed. White arrows represent sampling horizons for chemical analysis (scale: scraper 30 cm). **D:** Kitakaruizawa As–K pumice fall deposit. **E:** Tsumagoi, the Komoro 1 PDC deposit, overlain by the As–K pumice fall (view of As–K top obscured in the outcrops overhang shadow).

activity.

The isopach map for the As–K shows that the fall deposit was dispersed north-east of vent (Fig. 9A; Machida and Arai, 2003; Uesawa et al., 2022) yet Lake Suigetsu is positioned almost 250 km south-west of Asama. We therefore suggest that the fine-grained cryptotephra at Lake Suigetsu could be related to a co-PDC ash plume formed during the latter phases of the eruption, which could explain the dispersal away from the main dispersal axis (e.g., Engwell and Eychenne, 2016). Certainly, some of the most widespread Late Quaternary volcanic ash dispersals also have major distal components associated with a co-PDC ash transport mechanisms (e.g., Costa et al., 2014; Smith et al., 2016; Takarada and Hoshizumi, 2020). An As-UG co-PDC ash dispersal is also considered responsible for other Late-glacial Asama ash fall deposits traced offset from the two main Plinian dispersal axis, for instance As-UG is reported distally in western Tokyo, at Tachikawa (Machida and Suzuki, in press).

We re-analysed previously ascribed distal 'As–K' tephra layers preserved to the north-east in Sea of Japan (Table 5) cores GH89-2-22 (Nakajima et al., 1996) and YK10-07 PC09 (Nagahashi et al., 2022), along with the Ichi-no-Megata lake record northern Honshu (Okuno et al., 2011, Fig. 9A), and find they are all chemically similar to the

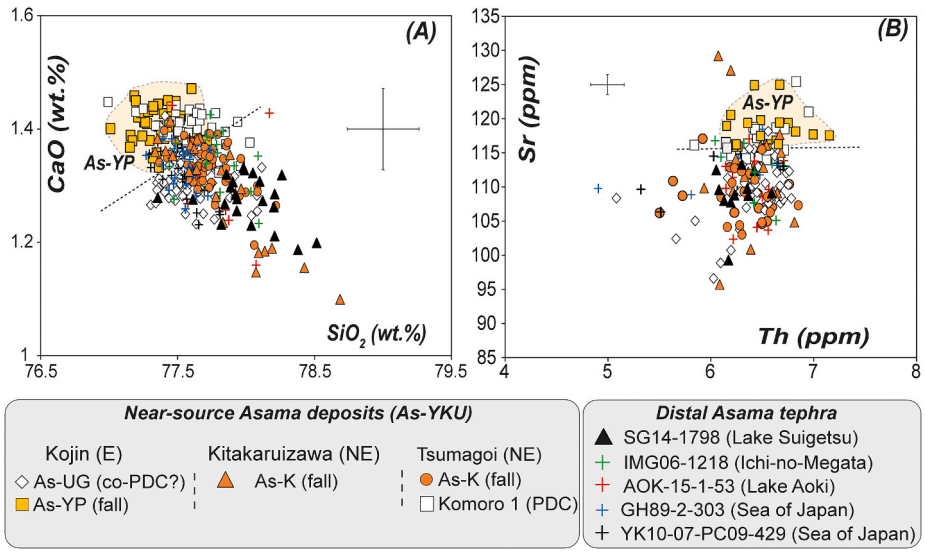


Fig. 10. Chemical comparison of Lake Suigetsu cryptotephra with near-source deposits and other distal occurrences of the As-YKU eruption **(A)** SiO_2 vs. CaO plot demonstrates that the As-YP (and Komoro PDC) glasses analysed tend to display subtly lower SiO_2 and higher CaO content than those of distal tephra SG14-1798, which is in turn is more consistent with the later As–K Plinian fall phase and the As-UG. **B:** Sr vs Th plot revealing that the As-YP pumice are again inconsistent with the distal Suigetsu tephra owing to higher Sr content, while the As–K and As-UG extend to lower Sr content consistent with SG14-1798.

second (As–K) Plinian phase (Fig. 10A and B) which is in agreement with their positions along the dominant north-east tephra dispersal (Fig. 9A), although from a chemical standpoint a contribution form the As-UG cannot be ruled out. Finally, we also report a new occurrence of a distal Late-glacial Asama tephra layer from a sediment core extracted from Lake Aoki (AOK-15-1; Table 5) at a CD of 52.5–53.0 cm. The 5 mm thick tephra (AOK-15-1-53) is stratigraphically positioned in the core above a 4.8 cm thick AT (CD 534.5–536.8 cm), and a 5 mm thick Daisen DHg (CD 488–488.5 cm) tephra layer, respectively. Glass chemical data verifying AT and DHg tephra tephrostratigraphic positions in AOK-15-1 are provided in the supplementary material 1 and Supplementary Fig. 4. AOK-15-1-53 has a variable composition, but it is largely consistent with the major element and trace element compositions of the SG14-1798 glasses, and the near-vent As–K and As-UG deposits.

In an attempt to better understand the timing of eruptive phases at Asama, we integrate the near-source and distal age information associated with the Asama-YKU eruption. The initial Plinian As-YP phase is ^{14}C dated based on tree stumps buried in the fall deposits (Nakamura et al., 1997), and multiple age determinations yield an age range of between 15,620–17,040 IntCal20 yrs BP (2σ). Charcoal from within the Komoro PDC are also ^{14}C dated (Yamada, 1997) and range from 16,230–16,840 IntCal20 yrs BP (2σ), which is consistent with the dating of the buried tree stumps found within As-YP (Fig. 8). Furthermore, the distal age of the 'As–K' tephra in the Ichi-no-Megata lake sediments northern Honshu (Okuno et al., 2011), is re-modelled to between 16,140–16,790 IntCal20 yrs BP (2σ), which is indistinguishable from the ages of the initial As-YP Plinian phase, and the associated Komoro PDC unit (Fig. 8).

SG14-1798 found in Lake Suigetsu, is chemically associated with the later phases of this Asama explosive activity, As–K and As-UG. The precise age of the cryptotephra at 16,545–16,695 IntCal20 yrs BP (2σ) is indistinguishable from the proximal dating of the earlier eruption phases (As-YP, As-Komoro PDC) suggesting that there was no significant temporal hiatus in the emplacement of this multi-phased eruptive sequence at Asama. This supports the proposed labelling of this multi-phased eruption as the As-YKU (Hayakawa, 2010; Machida and Suzuki, in press).

This multi-phased As-YKU eruption shows striking similarities with the albeit lower magnitude, andesitic, historical eruption of Asama in 1783 CE. The 1783 CE multi-phased eruption occurred over a three-month interval, depositing successive pumice fall deposits ESE, NE and NNW of the volcano, and these fall deposits are interbedded within PDC deposits found on the lower slopes of the volcano (Yasui and Koyaguchi, 2004). Importantly, the As-YKU tephra occurrence at Lake Suigetsu greatly increases the area of Honshu Island affected by ash fall from this multi-phased eruption, increasing from approximately 80,000 to 120,000 km^2. Our findings also highlight that the eruptive volume, and magnitude of this Asama eruption are likely to be poorly constrained.

The As-YKU eruption can be utilised as an effective chrono-stratigraphic marker across a very wide geographical and latitudinal range, linking sites from central and northern Honshu to those in the Sea of Japan (Fig. 9). Significantly, it occurs at an important climato-stratigraphic position close to the termination of the last glacial. Based on the Lake Suigetsu pollen-based temperature reconstruction (Nakagawa et al., 2021) the SG14-1798 (Asama-YKU) tephra is preserved in sediments relating to stadial conditions (SGPS-2), which are broadly equivalent to Greenland Stadial 2a (Fig. 7). The tephra also appears to be positioned within a period of local climatic instability prior to the overall warming that leads into the Late-glacial Interstadial (Fig. 7A). The direct synchronisation of Lake Suigetsu and Ichi-no-Megata climate records using the As-YKU offers future potential to assess time-transgressive climate change between central and northern Honshu during the last termination.

The Lake Suigetsu modelled age for SG14-1798, 16,619 ± 74 IntCal20 yrs BP (2σ), or 16,545–16,695 IntCal20 yrs BP (2σ), offers the most precise age for this isochron and is suitable for constraining the age-models of other sedimentary archives. Furthermore, this terrestrial based ^{14}C age estimate also offers excellent potential to accurately examine local ^{14}C marine reservoir offsets for the Sea of Japan sediments at the end of the last glacial, something that has been achieved in the Pacific Ocean using the To-H tephra (Ikehara et al., 2013). Our precise age for the As-YKU from Lake Suigetsu leaves little doubt that the Asama eruption is older than the To-H (15,615–15,895 IntCal20 yrs BP; Mueschler et al., 2020), which has remained unresolved because both widespread tephra deposits are not yet identified in the same stratigraphic succession. Finally, the As-YKU has been found in association with archaeological sites across the Kanto region, and thus our discovery offers improved chronological constraints, particularly in relation to the transition from microbifacial point and bifacial-stemmed points.

6.2.4. Kirishima volcanic complex (SG14-1806/Kr-Kb, and SG14-1185/Kr-St?)

Cryptotephra SG14-1806, dated at 16,789 ± 72 IntCal20 yrs BP (2σ), points to a source on Kyushu due to its high-K affinity and enrichment in Th and other incompatible trace elements (Figs. 4–6). We exclude Aso caldera as a potential source because erupted glass compositions display a higher K_2O trend at overlapping SiO_2 content relative to those of SG14-1806 (Fig. 4A). Instead, we consider a large magnitude 5.2 Plinian eruption (0.91 km^3) of the Karakunidake stratovolcano within the Kirishima volcanic complex, known as the Kirishima Kobayashi (Kr-Kb) tephra (Imura, 1992; Nagaoka et al., 2010) as a possible candidate. The Kr-Kb has an assigned age of ~16.7 ka based on it chrono-stratigraphic position within the Southern Kyushu tephrostratigraphic framework (Moriwaki et al., 2016). Major and trace element glass of SG14-1806 cryptotephra are consistent with Kr-Kb pumice fall (Table 4; Figs. 4–6). Based on the discovery of the Kr-Kb cryptotephra in Lake Suigetsu, the Kirishima Kobayashi eruption can be precisely dated at 16,789 ± 72 IntCal20 yr BP (2σ). This discovery extends the northern ash fall distribution associated with this Plinian activity, which was previously mapped to the east towards the Pacific coast where it is 5 cm thick (Nagaoka et al., 2010).

The Kr-Kb is positioned just below the As-YKU tephra in Lake Suigetsu, residing within the same overall climatic interval, unstable stadial conditions at the end of the last glacial (SGPS-2), and broadly contemporaneous with Greenland Stadial 2a. At Lake Suigetsu SG14-1806 appears to be positioned prior to the onset of a local warming trend (Fig. 7). From an archaeological standpoint, Kr-Kb represent an important regional tephra in Southern Kyushu. The switch from the use of knives to microblades in the region is associated with the cultural transition from Palaeolithic to Jomon archaeology (Moriwaki et al., 2016). Microblades are only reported from stratigraphically above the Kr-Kb tephra making this a useful, and now precise chronological marker for this cultural change in Kyushu.

Glass analyses of Kr-Kb near-source deposits confirm that the Kirishima complex, which comprises multiple small stratovolcanoes and pyroclastic cones (including Onamiike, Iimoriyama, Karakunidake, Koshikidake and Shinmoedake) is another source region of HKCA tephra units in Kyushu, something that was not obvious from available whole-rock datasets. Interestingly, a previously unassigned early Holocene Lake Suigetsu cryptotephra, SG14-1185, reported by McLean et al. (2018) has similar HKCA major and trace element glass compositions to the SG14-1806/Kr-Kb tephra (Fig. 4; Fig. 6). Consequently, SG14-1185 is likely to also be from a Kirishima edifice. The SG14-1185 tephra is dated at 9337 ± 34 IntCal20 yr BP (2σ) using the Lake Suigetsu chronology, which is broadly consistent with two known eruptions of the active Shinmoedake volcano located centrally within the Kirishima complex (Moriwaki et al., 2016). Firstly, a pumice fall deposits known as the Setao (Kr-St; ~10.4 ka), and secondly a scoria fall deposits called the Kamamuta (Kr-km; 8.1 ka). Neither are directly dated, and both have been assigned age estimates based on chrono-stratigraphy. Further chemical analysis of these units could help further constrain the timing of explosive eruptions within the Kirishima volcanic complex.

6.3. An integrated chrono-stratigraphic framework of Japanese volcanism and the timing of eruptive activity

The cryptotephra investigation here spanning the Late-glacial to early Holocene sediments of Lake Suigetsu acts to further strengthen the position of this unique sedimentary archive as the central node in the tephrostratigraphic framework of East Asia (Smith et al., 2013; McLean et al., 2018, 2020a, 2020b; Albert et al., 2018; 2019). Prior to this contribution ash fall events recorded in Lake Suigetsu had been linked to 14 different volcanoes, predominately from Japanese arc volcanoes, extending from Kyushu to Hokkaido, but also the intra-plate volcanoes of Ulleungdo and Changbaishan. Here we report ash fall from four additional source volcanoes, Sakurajima, Kirishima (Karakunidake), Asama and Niijima, further facilitating the integration of the regional tephrostratigraphic frameworks. Four of the five cryptotephra layers identified have been linked to known eruptions with Magnitudes of 4.0 (or VEI 4) and above. SG14-1554 is the only cryptotephra deposit that has not yet been assigned to a specific eruption unit, although it likely derives from Sakurajima volcano. Occurrences of ash fall in central Honshu (Lake Suigetsu) associated with magnitude 4 or greater eruptions from sources in Southern Kyushu, such as Sakurajima, are consistent with historical observations. For instance, ash deposition from the Taisho 1914 CE VEI 4 Plinian eruption was recorded across Kyushu, Shikoku, south-west and central Honshu, and even as far north as Sendai (Rahadianto et al., 2022). This acts to reinforce the importance of the sediments of Lake Suigetsu for providing minimum estimates on the reoccurrence interval of ash fall events associated with Magnitude 4 or greater eruptions at Kyushu volcanoes upwind of the lake.

Where the cryptotephra is robustly linked to a source eruption the exceptional ^{14}C and varve chronology of the Lake Suigetsu archive has dramatically improved the age estimates of these eruptions (Fig. 8). Reliable eruption ages are essential for accurately constraining the tempo of pre-historic volcanic activity, the reoccurrence intervals of hazardous ashfall events, and enabling more accurate magnitude-frequency assessments. In the case of Asama-YKU, we clearly highlight the importance of integrating proximal and distal chronological information from multiple sites to gain the most accurate assessment of the timing and dispersal of multi-phased eruptions. Importantly, our improved eruption ages can be incorporated into regional near-vent tephrostratigraphic frameworks, and within the age-depth models of other distal sedimentary archives which contain the same tephra layers, thus improving age constraints for those Japanese eruption deposits that are not yet precisely dated. Finally, from a palaeoclimate and archaeological standpoint the refined eruption age estimates provide crucial chronological markers capable of directly synchronising and dating records of past climate, and cultural changes, thus improving our ability to resolve the driving mechanism and their interplay.

7. Conclusions

Cryptotephra investigations here focus on the intensely-dated (^{14}C, varved) sediments of the Lake Suigetsu (SG14 core) spanning the Late-glacial to early Holocene, sediments which reside between two visible tephra layers in the core, the Ulleungdo (U)-Oki (10.2 ka) and the Sambe 'Sakate' (Sambe-Md-fl; 19.6 ka). Major and trace element volcanic glass compositions of the cryptotephra deposits are used to assign provenance to chrono-stratigraphically relevant eruption units. Five new cryptotephra layers are identified within this time interval and relate to sub-Plinian to Plinian activities of volcanic sources in southern Kyushu, central Honshu and the Izu arc. Three cryptotephra are derived from Kyushu, two from Sakurajima (SG14-1337; SG14-1554) and a third from Karakunidake (Kirishima; SG14-1806), all offering important chronological constraints on Jomon cultural transitions in southern Japan.

An early Holocene cryptotephra, SG14-1337 dated at 10,623 ± 50 IntCal20 yrs BP (2σ) relates to the Plinian eruption of Sakurajima Sz-Tk-3 (Pumice 13), providing an important chronological marker for permanent Jomon housing in Kyushu. Intriguingly, the second cryptotephra with a similar Sakurajima-type composition, SG14-1554 dated at 12,922 ± 58 IntCal20 yrs BP (2σ), occurs immediately prior to the onset of stadial conditions at Lake Suigetsu, broadly equivalent to the North Atlantic Younger Dryas, or Greenland Stadial 1 (albeit their onsets are not precisely synchronous, and are claimed to have been driven by different mechanisms – Nakagawa et al., 2021). However, SG14-1554 is chemically inconsistent with the stratigraphically relevant Sakurajima Satsuma (Sz-S) Plinian fall deposits. The oldest Kyushu cryptotephra, SG14-1806 dated at 16,789 ± 72 IntCal20 yrs BP (2σ) is chemically linked to the Plinian Kirishima Kobayashi (Kr-Kb) eruption of Karakunidake volcano within the Kirishima volcanic complex. Cryptotephra, SG14-1579 dated here at 13,320 ± 64 IntCal20 yrs BP (2σ)

occurs during the Late-glacial Interstadial, and relates to activity at Niijima volcano (Izu Arc) and specifically the Miyatsika-yama (Nj-Mt) eruption.

The most significant discovery relates to cryptotephra SG14-1798 dated at 16,619 ± 74 IntCal20 yrs BP (2σ) which we link to the multi-phased Asama-YKU eruption. Chemically this cryptotephra is most akin to the second Plinian phase, As–K and the associated As-UG. This discovery greatly expands the distribution of ash fall from this eruptive episode at Asama volcano. The climato-stratigraphic position of the eruption deposit in the Lake Suigetsu sediments, towards the end of the last glacial, and within unstable stadial conditions broadly contemporaneous with Greenland Stadial 2a (albeit the timing of the termination in Greenland and Japan is asynchronous), means that it offers an important chrono- and climato-stratigraphic marker extending over much of central and northern Honshu island (Fig. 9), which is suitable for assessing the spatial variability in past climate change during this important climatic interval.

The unrivalled chronology of the Lake Suigetsu sediment record has dramatically constrained the timing of the above-mentioned Magnitude 4.0 or greater Late-glacial to early Holocene Japanese eruptions, whilst also reinforcing the importance of this site as a central node within a fully integrated tephrostratigraphic framework for East Asia. Furthermore, the findings highlight that Lake Suigetsu is uniquely placed to offer a comprehensive long-term repository of ash fall events impacting central Honshu (currently 32 visible and 39 cryptotephra layers), and is suitable for examining the reoccurrence intervals of these hazardous events on the region.

Author contributions

Paul Albert: Conceptualisation, fieldwork, SG14 Lake Suigetsu coring, cryptotephra extraction and chemical analysis, writing the manuscript, reviewing, and editing the manuscript. **Danielle McLean**: fieldwork, SG14 Lake Suigetsu coring, chemical analysis, editing and reviewing the manuscript. **Hannah Buckland**: fieldwork, chemical analysis, editing and reviewing the manuscript. **Takehiko Suzuki**: fieldwork, reviewing and editing the manuscript. **Gwydion Jones**: cryptotephra extraction and identification, reviewing and editing the manuscript. **Richard Staff**: SG14 lake coring, age-depth modelling, reviewing, and editing the manuscript. **Sophie Vineberg**: reviewing and editing the manuscript. **Ikuko Kitaba**: SG14 Lake Suigetsu coring, reviewing the manuscript. **Keitaro Yamada;** SG14 Lake Suigetsu and Lake Aoki coring, reviewing the manuscript. **Hiroshi Moriwaki**: fieldwork, reviewing and editing. **Daisuke Ishimura**: Lake Aoki coring, reviewing, and editing the manuscript. **Ken Ikehara**: marine tephra sampling, reviewing, and editing. **Christina Manning**: chemical analysis of tephra deposits, reviewing and editing. **Takeshi Nakagawa**: Conceptualisation, SG14 Lake Suigetsu coring, pollen analysis, reviewing and editing manuscript. **Victoria Smith**: Conceptualisation, SG14 Lake Suigetsu coring, chemical analysis of tephra deposits, reviewing and editing the manuscript.

Declaration of competing interest

The authors declare that they have no known competing financial interests or personal relationships that could have appeared to influence the work reported in this paper.

Data availability

Data will be made available on request.

Acknowledgements

This research was funded through a UKRI Future Leaders Fellowship (FLF) award to P.G.A (MR/S035478/1) held at Swansea University. PGA also benefited from a Leverhulme Early Career Fellowship (ECF-2014-438) held at the University of Oxford. D.M, G.J and H.M.B contributions were also supported by the UKRI FLF. V.C.S was partly funded from the University of Oxford John Fell fund, and V.C.S and T.N acknowledge funding from the Japan Society for the Promotion of Science (JSPS; KAKENHI-15H021443). The Fukui-SG14 sediment coring campaign was funded by the Fukui Prefectural Government, and the coring was conducted by the team of Seibushisui Co. Ltd. Japan, led by A. Kitamura. The authors would like to thank Prof. Hiroshi Machida and Prof. Jun-Ichi Kimura for the provision of some reference samples and fruitful discussions. We also thank the Sakurajima Volcano Research Center, of the Disaster Prevention Research Institute of Kyoto University, and Professor Kazuhiko Kano (formerly Kagoshima University) for the provision of the Moeshima Island core tephra sample. Finally, we would like to thank Chunqing Sun, and an anonymous reviewer for their careful and constructive comments.

Appendix A. Supplementary data

Supplementary data to this article can be found online at https://doi.org/10.1016/j.quascirev.2023.108376.

References

Adolphi, F., Bronk Ramsey, C., Erhardt, T.R., Edwards, L., Cheng, H., Turney, C.S.M., Cooper, A., Svensson, A., Rasmussen, S.O., Fischer, H., Muscheler, R., 2018. Connecting the Greenland ice-core and U/Th timescales via cosmogenic radionuclides: testing the synchroneity of Dansgaard-Oeschger event. Clim. Past 14, 1755–1781. https://doi.org/10.5194/cp-14-1755-2018.

Albert, P.G., Smith, V.C., Suzuki, T., Tomlinson, E.L., Nakagawa, T., McLean, D., Yamada, M., Staff, R.A., Schlolaut, G., Takemura, K., Nagahashi, Y., Kimura, J.-I., Suigetsu 2006 Project Members, 2018. Constraints on the frequency and dispersal of explosive eruptions at Sambe and Daisen volcanoes (South-West Japan Arc) from the distal Lake Suigetsu record (SG06 core). Earth Sci. Rev. 185, 1004–1028. https://doi.org/10.1016/j.earscirev.2018.07.003.

Albert, P.G., Tomlinson, E.L., Lane, C.S., Wulf, S., Smith, V.C., Coltelli, M., Keller, J., Lo Castro, D., Manning, C.J., Müller, W., Menzies, M.A., 2013. Late Glacial explosive activity on Mount Etna: implications for proximal-distal tephra correlations and the synchronisation of Mediterranean archives. J. Volcanol. Geoth. Res. 265, 9–26. https://doi.org/10.1016/j.jvolgeores.2013.07.010.

Albert, P.G., Hardiman, M., Keller, J., Tomlinson, E.L., Smith, V.C., Bourne, A.J., Wulf, S., Zanchetta, G., Sulpizio, R., Müller, U.C., Pross, J., Ottolini, L., Matthews, I. P., Blockley, S.P.E., Menzies, M.A., 2015. Revisiting the Y-3 tephrostratigraphic marker: a new diagnostic glass geochemistry, age estimate, and details on its climatostratigraphical context. Quat. Sci. Rev. 118, 105–121. https://doi.org/10.1016/j.quascirev.2014.04.002.

Albert, P.G., Smith, V.C., Suzuki, T., McLean, D., Tomlinson, E.L., Miyabuchi, Y., Kibata, I., Mark, D.F., Moriwaki, H., , SG06 Project Members, Nakagawa, T., 2019. Geochemical characterisation of the widespread Japanese tephrostratigraphic markers and correlations to the Lake Suigetsu sedimentary archive (SG06 core). Quat. Geochronol. 52, 103–131. https://doi.org/10.1016/j.quageo.2019.01.005 in press.

Alley, R.B., Marotzke, J., Nordhaus, W.D., Overpeck, J.T., Peteet, D.M., Pielke Jr., R.A., Pierrehumbert, R.T., Rhines, P.B., Stocker, T.F., Talley, L.D., Wallace, J.M., 2003. Abrupt climate change. Science 299 (5615), 2005–2010. https://doi.org/10.1126/science.1081056.

Anma, K., Nagaoka, M., Niwa, S., Sekimoto, K., Yoshikawa, M., Fujine, H., 1990. A geological survey for the study on neotectonic movement and geoenvironment of Lake suwa, nagano prefecture. Mem. Geol. Soc. Jpn. 36, 179–194.

Aoki, K., 2020. Major-element Compositions of Volcanic Glass Shard in Late Quaternary Tephra provided from the Asama Volcano in An-Naka and Tomioka Area, Gunma Prefecture, Central Japan, vol. 55. Geographical Reports of Tokyo Metropolitan University, pp. 1–11, 2020.

Blockley, S.P.E., Pyne-O'Donnell, S.D.F., Lowe, J.J., Matthews, I.P., Stone, A., Pollard, A. M., Turney, C.S.M., Molyneux, E.G., 2005. A new and less destructive laboratory procedure for the physical separation of distal glass tephra shards from sediments. Quat. Sci. Rev. 24, 1952–1960. https://doi.org/10.1016/j.quascirev.2004.12.008.

Bourne, A.J., Abbott, P.M., Albert, P.G., Cook, E., Pearce, N.J.G., Ponomareva, V., Svensson, A., Davies, S.M., 2016. Underestimated risks of recurrent long-range ash dispersal from northern Pacific Arc volcanoes. Nature Scientific Reports 6, 2983. https://doi.org/10.1038/srep29837.

Bronk Ramsey, C., 2008. Deposition models for chronological records. Quat. Sci. Rev. 27 (1–2), 42–60. https://doi.org/10.1016/j.quascirev.2007.01.019.

Bronk Ramsey, C., Lee, S., 2013. Recent and planned developments of the program OxCal. Radiocarbon 55, 720–730. https://doi.org/10.1017/S0033822200057878.

Bronk Ramsey, C., et al., 2012. A complete terrestrial radiocarbon record for 11.2 to 52.8 kyr B.P. Science 338, 370–374. https://doi.org/10.1126/science.1226660.

Bronk Ramsey, C., Heaton, T.J., Schlolaut, G., Staff, R.A., Bryant, C.L., Brauer, A., Lamb, H.F., Marshal, M.H., Nakagawa, T., 2020. Reanalysis of the atmospheric

radiocarbon calibration record from Lake Suigetsu, Japan. Radiocarbon 62 (4). https://doi.org/10.1017/RDC.2020.18. IntCal20: Calibration Issue.
Choi, T.J., Takahama, N., Urabe, A., 2002. Tephrochronology of late Pleistocene to Holocene strath terraces along the aburuma river of the niigata basin, Central Japan. The Quat. Res (Daiyonki-kenkyu) 41 (1), 45–51. https://doi.org/10.4116/jaqua.41.45.
Clarke, P.U., Pisias, N.G., Stocker, T., Weaver, A., 2002. The role of the thermohaline circulation in abrupt climate change. Nature 415 (6874), 8630869. https://doi.org/10.1038/415863a.
Costa, A., Smith, V.C., Macedonio, G., Matthews, N.E., 2014. The magnitude and impact of the Youngest Toba Tuff super-eruption. Front. Earth Sci. Sec Volcanology 2. https://doi.org/10.3389/feart.2014.00016.
Engwell, S., Eychenne, J., 2016. Contribution of fine ash to the atmosphere from plumes associated with pyroclastic density currents. Volcanic Ash – Hazard Observation 67–85. https://doi.org/10.1016/B978-0-08-100405-0.00007-0.
Geshi, N., Yamada, I., Matsumoto, K., Nishihara, A., Miyagi, I., 2020. Accumulation of rhyolite magma and triggers for a caldera-forming eruption of the Aira Caldera, Japan. Bull. Volcanol. 82, 44. https://doi.org/10.1007/s00445-020-01384-6.
Hayakawa, Y., 1985. Pyroclastic geology of Towada volcano. Bull Earthq Res Inst. Univ Tokyo 60, 507–592.
Hayakawa, Y., 2010. Hayakawa's 2000-year eruption database and one million year tephra database. http://www.hayakawayukio.jp/database. Updated March 2022.
Hirose, K., Nagahashi, Y., Nakazawa, N., 2014. Lithostratigraphy and dating of lacustrine sediments core (INW2012) from Lake inawashiro-ko, fukushima prefecture, Japan. The Quat. Res (Daiyonki-kenkyu) 53 (3), 157–173 (in Japanese with Eng. abstract).
Ikehara, K., Ohkushi, K., Noda, A., Danhara, T., Yamashita, Y., 2013. A new local marine reservoir correction for the last deglacial period in the Sanriku region, northwestern North Pacific, based on radiocarbon dates from the Towada-Hachinohe (To-H) tephra. Quat. Res. 52, 127–137.
Ikehara, K., Usami, K., Kanamatsu, T., Danhara, T., Yamashita, T., 2017. Three important Holocene tephras off the Pacific coast of the Tohoku region, Northeast Japan: implications for correlating onshore and offshore event deposits. Quat. Int. 456, 138–153. https://doi.org/10.1016/j.quaint.2017.08.022.
Imura, R., 1992. Eruptive History of Kirishima Volcano during the Past 22000 Years, vol. 27. Geographical Reports of Tokyo Metropolitan University, pp. 73–89.
Jochum, K.P., Stoll, B., Herwig, K., Willbold, M., Hofmann, A.W., Amini, M., Aarburg, S., Abouchami, W., Hellebrand, E., Mocek, B., Raczek, I., Stracke, A., Alard, O., Bouman, C., Becker, S., Dücking, M., Brätz, H., Klemd, R., de Bruin, D., Canil, D., Cornell, D., de Hoog, C., Dalpé, C., Danyushevsky, L., Eisenhauer, A., Gao, Y., Snow, J.E., Groschopf, N., Günther, D., Latkoczy, C., Guillong, M., Hauri, E., Höfer, H.E., Lahaye, Y., Horz, K., Jacob, D.E., Kasemann, S.A., Kent, A.J.R., Ludwig, T., Zack, T., Mason, P.R.D., Meixner, A., Rosner, M., Misawa, K., Nash, B.P., Pfänder, J., Premo, W.R., Sun, W.D., Tiepolo, M., Vannucci, R., Vennemann, T., Wayne, D., Woodhead, J.D., 2006. MPI-DING reference glasses for in situ microanalysis: 581 New reference values for element concentrations and isotope ratios. G-cubed 7 (2).
Kariya, Y., Sasaki, A., Arai, F., 1998. Latest quaternary marker tephras in mount tariappyo, Central Japan. J. Geogr. 107 (1), 92–103.
Kimura, J.-I., Nagahashi, Y., Satoguchi, Y., Chang, Q., 2015. Origins of felsic magmas in Japanese subduction zone: geochemical characterizations of tephras from caldera-forming eruptions <5Ma. Geochem. Geophys. Geosysts. 16, 2147–2174. https://doi.org/10.1002/2015GC005854.
Kitagawa, H., van der Plicht, J., 1998a. Atmospheric radiocarbon calibration to 45,000 yr B.P.: late Glacial fluctuations and cosmogenic Isotope production. Science 279, 1187–1190. https://doi.org/10.1126/science.279.5354.1187.
Kitagawa, H., van der Plicht, J., 1998b. A 40,000-year varve chronology from Lake Suigetsu, Japan; extending the (super 14) C calibration curve. Radiocarbon 40, 505–515. https://doi.org/10.1017/S0033822200018385.
Kitagawa, H., van der Plicht, J., 2000. Atmospheric radiocarbon calibration beyond 11,900 cal Bp from Lake Suigetsu laminated sediments. Radiocarbon 42, 370–381. https://doi.org/10.1017/S0033822200030319.
Kitagawa, H., Fukuzawa, H., Nakamura, T., Okamura, M., Takemura, K., Hayashida, A., Yasuda, Y., 1995. AMS 14C dating of varved sediments from lake Suigetsu, Central Japan and atmospheric 14C change during the Lake Pleistocene. Radiocarbon 37, 371–378. https://doi.org/10.1017/S0033822200030848.
Kobayashi, T., Tameike, T., 2002. History of eruptions and volcanic damage from Sakurajima Volcano, southern Kyushu, Japan. The Quaternary Research (Daiyonki-Kenkyu) 41, 269–278.
Kobayashi, M., Aoki, A., Murata, M., Mishizawa, F., Suzuki, T., 2020. Tephrostratigraphy and eruption history after the mikatsukayama event on niikima volcano, Izu islands, Japan. Volcano 65 (2), 21–40. https://doi.org/10.18940/kazan.65.2_21.
Kurokawa, T., 2002. On the cultural pioneering in the first part of initial Jomon period, southern Kyushu, Japan. The Quat. Res. (Daiyonki-kenkyu) 41 (4), 331–344 (in Japanese with Eng. abstract).
Kutterolf, S., Freundt, A., Perez, W., Morz, T., Schacht, U., Wehrmannm, Schmincke, H.-U., 2008. Pacific offshore record of Plinian arc volcanism in Central America: along-arc correlations. G-cubed 9 (2). https://doi.org/10.1029/2007GC001631.
Lane, C.S., Brauer, A., Blockley, S.P.E., Dulski, P., 2013. Volcanic ash reveals time-transgressive abrupt climate change during the Younger Dryas. Geology 41 (12), 1251–1254. https://doi.org/10.1130/G34867.1.
Lane, C.S., Cullen, V.L., White, D., Bramham-Law, C.W.F., Smith, V.C., 2014. Cryptotephra as a dating and correlation tool in archaeology. J. Archaeol. Sci. 42, 42–50. https://doi.org/10.1016/j.jas.2013.10.033.
Lowe, J., Barton, N., Blockley, S., Ramsey, C.B., Cullen, V.L., Davies, W., Gamble, C., Grant, K., Hardiman, M., Housley, R., Lane, C.S., Lee, S., Lewis, M., MacLeod, A., Menzies, M., Müller, W., Pollard, M., Price, C., Roberts, A.P., Rohling, E.J., Satow, C., Smith, V.C., Stringer, C.B., Tomlinson, E.L., White, D., Albert, P., Arienzo, I., Barker, G., Boric, D., Carandente, A., Civetta, L., Ferrier, C., Guadelli, J., Karkanas, P., Koumouzelis, M., Müller, U.C., Orsi, G., Pross, J., Rosi, M., Shalamanov-Korobar, L., Sirakov, N., Tzedakis, P.C., 2012. Volcanic ash layers illuminate the resilience of Neanderthals and early modern humans to natural Hazards. Proc. Natl. Acad. Sci. U. S. A. 109, 13532–13537. https://doi.org/10.1073/pnas.1204579109.
Machida, H., 1999. Quaternary widespread tephra catalogue in and around Japan: recent progress. The Quaternary Research (Daiyonki-Kenkyu) 38, 194–203.
Machida, H., Arai, F., 2003. Atlas of Tephra in Japan and its Surrounding Area, second ed. University of Tokyo Press, Tokyo.
Machida, H. and Suzuki, T. Atlas of Tephra in Japan and its Surrounding Area, (in press) third ed.. University of Tokyo Press, Tokyo (In Japanese, title translated)..
Marshall, M., Schlolaut, G., Nakagawa, T., Lamb, H., Brauer, A., Staff, R., Bronk Ramsey, C., Tarasov, P., Gotanda, K., Haraguchi, T., Yokoyama, Y., Yonenobu, H., Tada, R., Suigetsu 2006 Project Members, 2012. Anovel approach to varve counting using mXRF and X-radiography in combination with thin-section microscopy, applied to the Late Glacial chronology from Lake Suigetsu, Japan. Quat. Geochronol. 13, 70–80. https://doi.org/10.1016/j.quageo.2012.06.002.
McLean, D., Albert, P.G., Nakagawa, T., Staff, R., Suzuki, T., , Suigetsu 2006 Project Members, Smith, V.C., 2016. Identification of the Changbaishan 'Millennium' (B-Tm) eruption in the Lake Suigetsu (SG06) sedimentary archive, Japan: synchronisation of hemispheric-wide palaeoclimate archives. Quat. Sci. Rev. 150, 301–307. https://doi.org/10.1016/j.quascirev.2016.08.022.
McLean, D., Albert, P.G., Nakagawa, T., Suzuki, T., Staff, R.A., Yamada, K., Kitaba, I., , SG14 Project Members, Smith, V.C., 2018. Integrating the Holocene tephrostratigraphy for East Asia using a high-resolution cryptotephra study from Lake Suigetsu (SG14 core), central Japan. Quat. Sci. Rev. 183, 36–38. https://doi.org/10.1016/j.quascirev.2017.12.013.
McLean, D., Albert, P.G., Suzuki, T., Nakagawa, T., Kimura, J.-I., Chang, Q., Miyabuchi, Y., Manning, C.J., MacLeod, A., Blockley, S.P.E., Staff, R.A., Yamada, K., Kitaba, I., Yamasaki, A., Haraguchi, T., Kitagawa, J., , SG14 Project Members, Smith, V.C., 2020a. Constraints on the timing of explosive volcanism at Aso and Aira calderas (Japan) between 50 and 30 ka: new insights from the Lake Suigetsu sedimentary record (SG14 core). G-cubed 21 (8). https://doi.org/10.1029/2019GC008874.
McLean, D., Albert, P.G., Suzuki, T., Nakagawa, T., Kimura, J.-I., Chang, Q., Miyabuchi, Y., Manning, C.J., MacLeod, A., Blockley, S.P.E., Staff, R.A., Yamada, K., Kitaba, I., Yamasaki, A., Haraguchi, T., Kitagawa, J., Smith, V.C., 2020b. Refining the eruptive history of Ulleungdo and Changbaishan volcanoes (East Asia) over the last 86 kyrs using distal sedimentary records. J. Volcanol. Geoth. Res. 389, 106669 https://doi.org/10.1016/j.jvolgeores.2019.106669. SG14 Project Members.
McLean, D., Albert, P.G., Schlolaut, G., Lamb, H.F., Marshall, M.H., Brauer, A., Wade, J., Nakagawa, T., Smith, V.C., 2022. How reliable is μXRF core scanning at detecting tephra layers in sedimentary records? A case study using the Lake Suigetsu archive (central Japan). J. Quat. Sci. 37 (7), 1189–1206. https://doi.org/10.1002/jqs.3432.
Moriwaki, H., Suzuki, T., Murata, M., Ikehara, M., Machida, H., Lowe, D.J., 2011. Sakurajima-Satsuma (Sz-S) and Noike-Yumugi (N-Ym) tephras: new tephrochronological marker beds for the last deglaciation, southern Kyushu, Japan. Quat. Int. 246 (1–2), 203–212. https://doi.org/10.1016/j.quaint.2011.03.046.
Moriwaki, H., Nakamura, N., Nagasako, T., Lowe, D.J., Sangawa, T., 2016. The role of tephra in developing chronostratigraphy for palaeoenvironmental reconstruction and archaeology in southern Kyushu, Japan, since 30,000 cal. BP: an integration. Quat. Int. 397, 79–92. https://doi.org/10.1016/j.quaint.2015.05.069.
Moriwaki, H., Nagasako, T., Nishizawa, F., Matsushima, Y., Suzuki, T., Tanaka, G., 2017. Chronology and significance of marine deposits on Shinjima (Moeshima) island, Kagoshima Bay, based on tephrochronology and 14C ages. J. Geogr. 126, 557–579. https://doi.org/10.5026/jgeography.126.557.
Muscheler, R., Adophi, F., Heaton, T.J., Ramsey Svenson, A., van der Plicht, J., Reimer, P., 2020. Testing and improving the IntCal20 calibration curve with independent records. Radiocarbon 62 (4), 1979. https://doi.org/10.1017/RDC.2020.54, 1094.
Nagahashi, Y., Fukaya, M., Ikehara, K., Sagawa, T., 2022. Late Pleistocene to Holocene tephrastratigraphy in the off Wakasa Bay sediment cores and correlation with wide-spread tephras. Quat. Res. (Daiyonki-kenkyu) (in Japanese with Eng. abstract).
Nagaoka, S., Arai, F., Danhara, T., 2010. The past 600 ka explosive eruptive history of Kirishima volcano based on tephra layers in miyazaki plain, southern Japan. J. Geogr. 119 (1), 121–152 (in Japanese with Eng. abstract).
Nakagawa, T., Gotanda, K., Haraguchi, T., Danhara, T., Yonenobu, H., Brauer, A., Yokoyama, Y., Tada, R., Takemura, K., Staff, R.A., Payne, R., Bronk Ramsey, C., Bryant, C., Brock, F., Schlolaut, G., Marshall, M., Tarasov, P., Lamb, H., Suigetsu 2006 Project Members, 2012. SG06, a fully continuous and varved sediment core from Lake Suigetsu, Japan: stratigraphy and potential for improving the radiocarbon calibration model and understanding of late Quaternary climate changes. Quat. Sci. Rev. 36, 164–176. https://doi.org/10.1016/j.quascirev.2010.12.013.
Nakagawa, T., Tarasov, P., Staff, R.A., Bronk Ramsey, C., Marshall, M., Schlolaut, G., Bryant, C., Brauer, A., Lamb, H., Haraguchi, T., Gotanda, K., Kitaba, I., Kitagawa, H., van der Plicht, J., Yonenobu, H., Omori, T., Yokoyama, Y., Tada, R., Yasuda, Y., 2021. The spatio-temporal structure of the Lateglacial to early Holocene transition reconstructed from the pollen record of Lake Suigetsu and its precise correlation with other key global archives: implications for palaeoclimatology and archaeology. Global Planet. Change 202, 103493. https://doi.org/10.1016/j.gloplacha.2021.103493.
Nakagawa, T., Kitagawa, H., Yasuda, Y., Tarasov, P.E., Gotanda, K., Sawai, 2005. Pollen/event stratigraphy of the varved sediment of Lake Suigetsu, central Japan from 15,701 to 10,217 SG vyr BP (Suigetsu varve years before present): Description,

interpretation, and correlation with other regions. Quat. Sci. Rev. 24 (14–15), 1691–1701. https://doi.org/10.1016/j.quascirev.2004.06.022.
Nakagawa, T., Kitigawa, H., Yasuda, Y., Tarasov, P.E., Nishida, K., Gotanda, K., Sawai, Y., Yangtze River Civilisation Programme Members, 2003. Asynchronous climate changes in the North atlantic and Japan during the last termination. Science 299, 688–691.
Nakajima, T., Kikkawa, K., Ikehara, K., Katayama, H., Kikawa, E., Joshima, M., Seto, K., 1996. Marine sediments and late Quaternary stratigraphy in the southeastern part of the Japan Sea –Concerning the timing of dark layer deposition. Jour. Geol. Soc. Japan 102, 125–138 (in Japanese with Eng. abstract).
Nakamura, T., Tsuji, S., Takemoto, H., Ikeda, A., 1997. 14C age measurements with accelerator mass spectrometry of Asama tephra stratigraphic samples around Minami-Karuizawa, the latest Pleistocene, Nagano Prefecture, central Japan. J. Geol. Soc. Jpn. 103, 990–993 (in Japanese).
Nakamura, Y., Sugai, T., Ishihara, T., Freire, A.F., Matsumoto, R., 2013. Late Pleistocene tephrostratigraphy of sea-bottom sediments in the eastern margin of Japan by MD 179-Japan Sea gas hydrate expedition. J. Jpn. Assoc. Pet. Technol. 78 (1), 79–91 (In Japanese with English abstract).
Nakazawa, Y., Naganuma, M., Tsutsumi, T., 2022. The emergence and transmission of early pottery in the Late-Glacial Japan. Quat. Int. 608–609, 75–87. https://doi.org/10.1016/j.quaint.2021.02.037.
Noshiro, S., Suzuki, M., Tsuji, S., 2004. Latest Pleistocene forest buried by Asama tephra in the Minami-Karuizawa basin, central Japan. Jpn. J. Histor. Bot. 13 (1), 13–23.
Okuno, M., 1997. Accelerator Mass Spectrometric Radiocarbon Chronology during the Last 30,000 Years of the Aira Caldera, Southern Kyushu, Japan, vol. 8. Summaries of Researches Using AMS at Nagoya University, pp. 183–221, 1997.
Okuno, M., Nakamura, T., Moriwaki, H., Kobayashi, T., 1997. AMS radiocarbon dating of the Sakurajima tephra group, Southern Kyushu, Japan. Nucl. Instrum. Methods Phys. Res. B 123, 470–474. https://doi.org/10.1016/S0168-583X(96)00614-3.
Okuno, M., Tameike, T., Naruo, H., Moriwaki, H., Nakamura, T., Kobayashi, T., 1999. Eruption age of P13 tephra (Sz-P13) from Sakurajima volcano based on AMS 14C dates of buried soils, 1999 Kagoshima-Koko 33 (Special issue), 95–102 (in Japanese).
Okuno, M., Torii, M., Yamada, K., Shinozuka, Y., Danhara, T., Gotanda, K., Yonenobu, H., Yasuda, Y., 2011. Widespread tephras in sediments from lake Ichi-no-Megata in northern Japan: Their description, correlation and significance. Quat. Int. 246 (1–2), 270–277. https://doi.org/10.1016/j.quaint.2011.08.015.
Pearson, R., 2006. Jomon hot spot: increasing sedentism in south-western Japan in the Incipient Jomon (14,000–9250 cal. BC) and Earliest Jomon (9250–5300 cal. BC) periods. Sedentism in non-agricultural societies 38 (2), 239–258. https://doi.org/10.1080/00438240600693976. World Archaeology.
Peccerillo, A., Taylor, S.R., 1976. Geochemistry of eocene calc-alkaline volcanic rocks from the Kastamonu area, Northern Turkey. Contrib. Mineral. Petrol. 58 (1), 63–81, 1976.
Rahadianto, H., Tatano, H., Iguchi, M., Tanaka, H.L., Takemi, T., Roy, S., 2022. Long-term ash dispersal dataset of the Sakurajima Taisho eruption for ashfall disaster countermeasure. Earth Syst. Sci. Data 14, 5309–5332. https://doi.org/10.5194/essd-14-5309-2022.
Reimer, P., Austin, W., Bard, E., Bayliss, A., Blackwell, P., Bronk Ramsey, C., Talamo, S., 2020a. The IntCal20 northern hemisphere radiocarbon age calibration curve (0–55 cal kBP). Radiocarbon 62 (4), 725–757. https://doi.org/10.1017/RDC.2020.41.
Reimer, P.J., Austin, W.E.N., Bard, E., Bayliss, A., Blackwell, P.G., Bronk Ramsey, C., Butzin, M., Cheng, H., Edwards, R.L., Friedrich, M., Grootes, P.M., Guilderson, T.P., Hajdas, I., Heaton, T.J., Hogg, A.G., Hughen, K.A., Kromer, B., Manning, S.W., Muscheler, R., Palmer, J.G., Pearson, C., van der Plicht, J., Reimer, R.W., Richards, D.A., Scott, E.M., Southon, J.R., Turney, C.S.M., Wacker, L., Adophi, F., Büntgen, U., Capano, M., Fahrni, S., Fogtmann-Schulz, A., Friedrich, R., Kudsk, S., Miyake, F., Olsen, J., Reinig, F., Sakamoto, M., Sookdeo, A., Talamo, S., 2020b. The IntCal20 Northern Hemisphere radiocarbon calibration curve (0–55 cal kBP). Radiocarbon 62 (4), 725–757. https://doi.org/10.1017/RDC.2020.41.
Schlolaut, G., Marshall, M., Brauer, A., Nakagawa, T., Lamb, H., Staff, R., Bronk Ramsey, C., Bryant, C., Brock, F., Kossler, A., Tarasov, P., Yokoyama, Y., Tada, R., Haraguchi, T., Suigetsu 2006 Project Members, 2012. An automated method for varve interpolation and its application to the Late Glacial chronology from Lake Suigetsu, Japan. Quat. Geochronol. 13, 52–69. https://doi.org/10.1016/j.quageo.2012.07.005.
Schlolaut, G., Brauer, A., Nakagawa, T., Lamb, H.F., Tyler, J.J., Staff, R.A., Marshall, M. H., Bronk Ramsey, C., Bryant, C.L., Tarasov, P.E., 2017. Evidence for a bi-partition of the younger Dryas stadial in East Asia associated with inversed climate characteristics compared to europe. Sci. Rep. 7, 44983 https://doi.org/10.1038/srep44983.
Schlolaut, G., Staff, R., Brauer, A., Lamb, H.F., Marshall, M.H., Bronk Ramsey, C., Nakagawa, T., 2018. An extended and revised Lake Suigetsu varve chronology from ~ 50 to ~ 10 ka BP based on detailed sediment micro-facies analyses. Quat. Sci. Rev. 200, 351–366. https://doi.org/10.1016/j.quascirev.2018.09.021.
Smith, V.C., Mark, D.F., Staff, R.A., Blockley, S.P.E., Bronk Ramsey, C., Bryant, C.L., Nakagawa, T., Kyu Han, K., Weh, A., Takemura, K., Danhara, T., 2011. Toward establishing precise 40Ar/39Ar chronologies for Late Pleistocene palaeoclimate archives: an example from the Lake Suigetsu (Japan) sedimentary record. Quat. Sci. Rev. 30 (21–22), 2845–2850. https://doi.org/10.1016/j.quascirev.2011.06.020. Suigetsu Project Members.
Smith, V.C., Staff, R.A., Blockley, S.P.E., Bronk Ramsey, C., Nakagawa, T., Mark, D.F., Takemura, K., Danhara, T., 2013. Identification and correlation of visible tephras in the Lake Suigetsu SG06 sedimentary archive, Japan: chronostratigraphic markers for synchronising of east Asian/west Pacific palaeoclimatic records across the last 150 ka. Quat. Sci. Rev. 67, 121–137. https://doi.org/10.1016/j.quascirev.2013.01.026. Suigetsu Project Members.
Smith, V.C., Isaia, R., Engwell, S., Albert, P.G., 2016. Tephra dispersal during the Campanian Ignimbrite (Italy) eruption: implications for ultra-distal ash transport during the large caldera-forming eruption. Bull. Volcanol. 78, 45. https://doi.org/10.1007/s00445-016-1037-0.
Staff, R.A., Bronk Ramsey, C., Bryant, C.L., Brock, F., Payne, R.L., Schlolaut, G., Marshall, M.H., Brauer, A., Lamb, H.F., Tarasov, P.E., Yokoyama, Y., Haraguchi, T., Gotanda, K., Yonenobu, H., Nakagawa, T., Suigetsu 2006 Project Members, 2011. New C-14 determinations from Lake Suigetsu, Japan: 12,000 to 0 cal BP. Radiocarbon 53, 511–528. https://doi.org/10.1017/S0033822200034627.
Staff, R.A., Nakagawa, T., Schlolaut, G., Marshall, M.H., Brauer, A., Lamb, H.F., Bronk Ramsey, C., Bryant, C.L., Brock, F., Kitagawa, H., van der Plicht, J., Payne, R.L., Smith, V.C., Mark, D.F., MacLeod, A., Blockley, S.P.E., Schwenninger, J., Tarasov, P. E., Haraguchi, T., Gotanda, K., Yonenobu, H., Yokoyama, Y., Suigetsu 2006 Project Members, 2013a. The multiple chronological techniques applied to the Lake Suigetsu (SG06) sediment core. Boreas 42 (2), 259–266. https://doi.org/10.1111/j.1502-3885.2012.00278.x.
Staff, R.A., Schlolaut, G., Bronk Ramsey, C., Bronk, F., Bryant, C.L., Kitagawa, H., van der Plicht, J., Marshall, M.H., Brauer, A., Lamb, H.F., Payne, R.L., Tarasov, P.E., Haraguchi, T., Gotanda, K., Yonenobu, Y., Nakagawa, T., 2013b. Integration of the old and new Lake Suigetsu (Japan) terrestrial radiocarbon calibration data sets. Radiocarbon 55 (4), 2049–2058. https://doi.org/10.2458/azu_js_rc.v55i2.16339.
Steffensen, J.P., Andersen, K.K., Bigler, M., Clausen, H.B., Dahl-Jensen, D., Fischer, H., Goto-Azuma, K., Hansson, M., Johnsen, S.J., Jouzel, J., Masson-Delmotte, V., Popp, T., Rasmussen, S.O., Röthlisberger, R., Ruth, U., Stauffer, B., Siggaard-Andersen, M.-L., Sveinbjörnsdóttir, A.E., Svensson, A., White, J.W.C., 2008. High-resolution Greenland ice core data show abrupt climate change happens in few years. Science 321 (5889), 680–684. https://doi.org/10.1126/science.1157707.
Sulpizio, R., Zanchetta, G., Caron, B., Dellino, P., Mele, D., Giaccio, B., Insinga, D., Paterne, M., Siani, G., Costa, A., Macedonio, G., Santacroce, R., 2014. Volcanic ash hazard in the Central Mediterranean assessed from geological data. Bull. Volcanol. 76, 866. https://doi.org/10.1007/s00445-014-0866-y.
Sun, S., McDonough, W.F., 1989. Chemical and isotopic systematics of 630 oceanic basalts: implications for mantle composition and processes. In: Saunders, A.D., Norry, M.J. (Eds.), Magmatism in Ocean Basins, 631.
Sun, C., Plunkett, G., Liu, J., Hongli, Z., Sigl, M., McConnell, R., Pilcher, J.R., Vinther, B., Steffensen, J.P., Hall, V., 2014. Ash from the Changbaishan Millennium eruption recorded in the Greenland ice: implications for determining the eruption's timing and impact. Geophys. Res. Lett. 41 (2), 694–701. https://doi.org/10.1002/2013GL058642.
Sun, C., Wang, L., Plunket, G., Zhang, E., Liu, J., 2021. An integrated late Pleistocene to Holocene tephrostratigraphic framework for south-east and east Asia. Geophys. Res. Lett. 48 (5) https://doi.org/10.1029/2020GL090582.
Suzuki, T., 1990. Tephra Layers in the Coastal Region of North Kanto and Their Related Problems, vol. 3. Kanto-Heiya, pp. 23–32.
Suzuki, T., 1991. Quaternary tephra studies in the Kanto-Chuba districts central Japan, Significance of middle Plieistocene tephra layers. The Quat. Res. (Daiyonki-kenkyu) 30, 361–368 (in Japanese with Eng. abstract).
Suzuki, T., 1993. Stratigraphy of middle Pleistocene tephra layers around nasuno plain, in north Kanto, Central Japan. J. Geogr. 102 (1), 73–90 (in Japanese, English abstract).
Takarada, S., Hoshizumi, H., 2020. Distribution and eruptive volume of aso-4 pyroclastic density current and tephra fall deposits, Japan: a M8 super-eruption. Front. Earth Sci. 23 https://doi.org/10.3389/feart.2020.00170.
Takemoto, H., 1996. Ookuwa debris avalanche deposit and the tephra layers of the Hotokeiwa and Maetake stage. Quat. Res. 40th Anniversary Special. In: Inventory of Quaternary Outcrops Tephras in Japan. Japan. Assoc, p. 182 (J).
Tomlinson, E.L., Thordarson, T., Muller, W., Thirlwall, M., Menzies, M.A., 2010. Microanalysis of tephras by LA-ICP-MS- strategies, advantages and limitations assessed using the Thorsmork ignimbrite (Southern Iceland). Chem. Geol. 279, 73–89. https://doi.org/10.1016/j.chemgeo.2010.09.013.
Tsuji, S., 1996. Maebashi peat formation on the maebashi plateau: transition from paleoloecolgical environment of the last glacial period to post glacial. Assoc. Quat. Res. 40th anniversary special. In: Inventory of Quaternary Outcrops Tephras in Japan, p. 184 (J).
Tsuji, S., Miyaji, N., Arai, F., 2004. Tephrostratigraphy and chronology of Asama volcano at Minami-Karuizawa as a basis of studies on environmental and disaster history. Bulletin of the National Museum of Japanese History No 118, 165–192 (in Japanese).
Turney, C.S.M., 1998. Extraction of rhyolitic component of Vedde microtephra from minerogenic lake sediments. J. Paleolimnol. 19, 199–206.
Uesawa, S., Toshida, K., Takeuchi, S., Miura, D., 2022. Creating a digital database of tephra fallout distribution and frequency in Japan. Journal of Applied Volcanology 11, 14. https://doi.org/10.1186/s13617-022-00126-x.
Yamada, O., 1997. KSU radiocarbon dates II. Radiocarbon 39 (1), 89–113.
Yasui, M., Koyaguchi, T., 2004. Sequence and eruptive style of the 1783 eruption of Asama Volcano, central Japan: a case study of an andesitic explosive eruption generating fountain-fed lava flow, pumice fall, scoria flow and forming a cone. Bull. Volcanol. 66, 243–262. https://doi.org/10.1007/s00445-003-0308-8.
Yoshida, H., Sugai, T., 2005. Impact of "24 ka nakanojo mud flow" event on the fluvial landform development in nakanojo basin, Central Japan. The Quat. Res. (Daiyonki-kenkyu) 44 (1), 1–13 (in Japanese with Eng. abstract).